On the Development and Application of Hybrid Numerical Models in Nonlinear Free Surface Hydrodynamics *

Stéphan T. Grilli
University of Rhode Island, Depart. of Ocean Engng., Narragansett, RI 02882.

Abstract

In this article, we report on the development of hybrid numerical models used to simulate free surface, i.e., wave, hydrodynamics, wave-structure interactions, wave breaking and nearshore transformation, and wave-induced sediment transport. Specifically, a two- (2D) or three-dimensional (3D) numerical wave tank (NWT), based on Fully Nonlinear Potential Flow (FNPF) equations, is used to simulate fully nonlinear wave generation and propagation from the far-field to the near-field, where a Navier-Stokes (NS) model is coupled with or nested within the NWT, to simulate near-field phenomena of more complex physics. In one presented application, a 2D-NWT is used to simulate periodic or irregular incident waves whose kinematics forces simulations of flow and sediment transport over the seabed and around partially buried obstacles. The suspended sediment transport is modeled in the near field in the NS model, using an immersed-boundary method and an embedded sediment transport model. Turbulence is represented by Large Eddy Simulation (LES) in the NS model, with a subgrid dynamic Smagorinsky scheme. The 2D- and 3D-NWTs are based on a higher-order Boundary Element Method (BEM), with an explicit second-order time stepping. Hence, only the NWT boundary is discretized. The solution for the velocity potential and its derivatives along the boundary is obtained in the BEM, which subsequently provides a solution at any required internal point within the domain. The NS-LES model domain is both initialized and driven for later time by the three-dimensional velocity field computed in the NWT. In the present formulation, the total velocity and pressure fields are expressed as the sum of irrotational (incident/far-field) and near-field viscous perturbations. The NS equations are formulated and solved for the perturbation fields, which are forced by the incident fields computed in the NWT. The feasibility of coupling the irrotational flow and NS solutions in an efficient hybrid manner is demonstrated.

1. INTRODUCTION

Recent progress made in the solution of fully nonlinear free surface flows, over complex bottom topography and around structures, combined with the increasing power and affordability of large computer clusters, have made it increasingly feasible predicting parameters of complex flows, with an accuracy and a resolution approaching that expected from experiments performed in large scale laboratory wave tanks. For this reason, such computer models are often referred to as Numerical Wave Tank (NWT), a term coined some 20 years ago [52], at a time when NWTs were only the dream of a distant future.

Nevertheless, as usual with any step increase in model performance and/or computing power, it is customary for scientists and engineers to immediately formulate a problem that pushes current resources to the limit, or even is beyond the reach of those. Hence, ever since computer models were invented and put in operation, for optimum efficiency, one has always tried to limit the model

*Keynote lecture published in *Proc. 8th Intl. Conf. on Hydrodynamics* (Nantes, France, September 2008) (P. Ferrant and X.B. Chen, eds.), pps. 21-50. ICHD2008 Local Organizing Committee Publications.

"physics" (i.e., such as represented in its equations and boundary conditions) to that *necessary and sufficient* for solving a given problem. This might mean, when the physics permits it, for some problems, that one can assume an incompressible, inviscid, or even irrotational fluid flow, while for other cases, one needs to deal with possibly compressible and fully viscous, or even multi-phase, fluid flows.

For problems with multiple scales or large inhomogeneities in model domain geometry and/or nature, however, the required physics might turn out to be different for different parts of the computational domain and one is faced with either using the more accurate physics everywhere (a costly choice) or somehow adapting such physics to the nature of the problem, in various parts of the computational domain. The latter is best achieved through model coupling or, even better, through using a hybrid model. Although differences between those might appear minor to most, in this author's mind, coupled models are those where one model (with given physics) simply passes information (in the form of flow kinematics and/or dynamics) to another model (with another physics and/or different scales of representation), through boundary conditions, along "matching" boundaries, and/or initialization of one model by another. Coupled models are thus run and operated independently from each other and the passing of information can simply be effected through the equivalent of shared data files. Furthermore, in coupled models, information will usually only travel one way, i.e., without feedback from the second model into the first one. By contrast, in *hybrid models* both model's equations and numerical procedures are truly integrated with each other and, if necessary, feedback from the second model onto the first one may be simulated.

An example of the *coupled model* approach, in this author's experience, for instance, is the computations of tsunami sources, by solving either half-plane elasticity equations for a sub-bottom dislocation (in a subduction zone), in the case of co-seismic tsunamis [21, 51, 73], or by performing full two- (2D) or three- (3D) dimensional simulations of (strongly nonlinear) flow generated by submarine or subaerial landslides, for landslide tsunamis [1, 2, 21, 27, 28, 36, 37, 60, 63, 64, 81, 93, 100, 101]. Such a source may initially correspond to very complex 3D waves but due to the nature of such problems will rapidly appear as a series of long-wave trains, radiating away from the source, when moving away from the later ("throw the pebble in the pond" analogy). Hence, source information might ultimately be best moved, for further computations, into a *coupled* 2D-horizontal depth-integrated long wave model, for propagation over ocean scales (such as represented by Linear or Nonlinear Shallow Water or Boussinesq equations [102]). This would require depth-integration of the source 3D flow fields and re-interpolation onto the 2D long wave model grid, a series of tasks that are in fact quite trivial. When approaching the coast, long tsunami-wave trains may then encounter ocean and coastal structures and eventually a sloping beach on which shoaling, breaking, inundation and runup will occur. The accurate prediction of tsunami forces and impact on structures as well as inundation and runup, over much smaller length scales than those of transoceanic propagation, might now require using other types of "nested" models, including finer coastal grids for long-wave models, even finer and different types of inundation models, as well as 3D and fully viscous wave-structure interaction models in the near field surrounding specific structures, making thus for quite challenging simulations [19].

Another example of coupled model approach is found in free surface hydrodynamics, as related to more traditional wave mechanics. Indeed, once generated, surface gravity waves closely behave as irrotational inviscid flows, well simulated by potential flow theory or other derived set of equations (e.g., [102]) up to wave overturning [24, 46, 58, 59, 66, 67, 84]. [Note, when using fully nonlinear free surface boundary conditions, one refers to these models as "Fully Nonlinear Potential Flow" models (FNPF).] The interaction of waves with ocean or coastal structures, and the beach, leading to flow separation and/or breaking, however, requires using more complex viscous/turbulent models, with a free surface representation that further allow for the representation of breaking waves beyond overturning (e.g., as provided in a Volume Of Fluids (VOF) approach; e.g.,

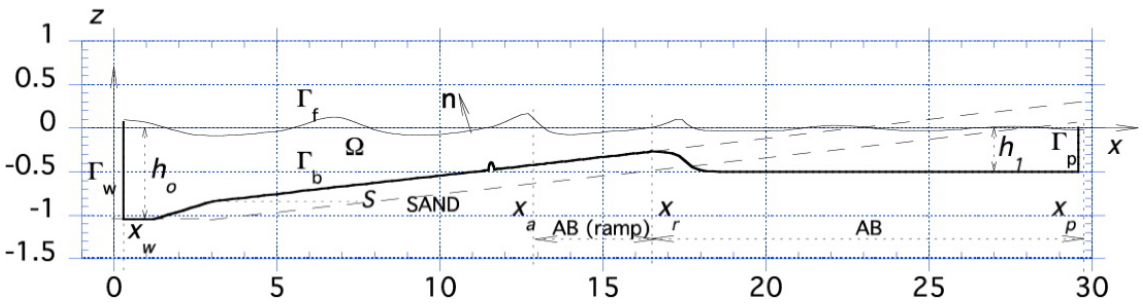

Figure 1: Sketch of a 2D-NWT used for wave shoaling and breaking simulations, over a $S = 1 : 24$ slope. Energy dissipation due to friction or breaking is specified over the (sandy) slope (for $x \leq x_r$) and in an absorbing beach (AB, for $x \geq x_a$); a piston wavemaker is located at $x = x_w$. (— —) indicates the position of the sand layer in the laboratory wave tank used at ASU, for which dimensions are in meters [61, 62]; in these experiments, there was a 8.4 cm radius, 50% buried, cylinder at $x = 12.8$ m.

Lin and Liu [80], Lubin [83]). Such models typically solve 3D Navier-Stokes (NS) equations over fine grids, and are thus very computationally intensive. They may also suffer from excessive numerical dissipation over long distances of propagation, implying that incident gravity waves would dissipate their energy in an excessive non-physical manner when propagated in large domains, for such models. For this reason, over the past 10 years, Grilli and co-workers have been involved in the development of coupled (and hybrid) FNPF-NS-VOF models in 2D [46, 65, 66, 72, 77] and 3D [4,17], to study wave shoaling and breaking on slopes and beaches, and wave-structure interactions. In these problems, incident waves generated and propagated in the FNPF model were either long extreme waves, such as FNPF solitary waves [94] or generated long waves [44], or extreme periodic waves (a.k.a., freak waves) generated in a 3D-NWT through directional focusing [7,8,35].

More recently, a 2D-FNPF/3D-NS hybrid model was developed to study wave-induced sediment transport and scouring around bottom obstacles [43, 48]. Fig. 1, for instance shows a sketch for far-field wave generation in a 2D-NWT, and propagation over a sloping bottom, up to close to breaking (before dissipation in an absorbing beach). A small half-buried cylinder is located on the bottom, just before the surfzone and the model is used to compute forcing wave fields around such a bottom obstacles, to be used in a coupled 3D-NS model, with embedded sediment transport computation.

In the following, after a brief survey of the state of the art in NWTs, we detail various formulations used in coupled and hybrid models developed by Grilli ad co-workers, and present a few typical applications of these. This includes a summary of governing equations, boundary conditions, and an overview of numerical methods for each model.

2. NWTS FOR THE MODELING OF NONLINEAR WAVES

In parallel with the continuous improvements of experimental wave facilities, recent progress in the development and application of so-called "Numerical Wave Tank" (NWT), combined with the power of large computer clusters, have made it increasingly possible to accurately and efficiently model complex wave and wave-structure interaction processes, such as routinely tested in the laboratory. These include wave generation, propagation, and interaction of non-breaking and breaking waves with a beach or ocean structures (submerged, bottom mounted/surface piercing, or floating). Due to the various geometric scales involved in such processes and the nature of incident waves of interest (typically intermediate to long), it is anticipated that wave processes should be adequately resolved in a NWT whose discretization has a ∼10-20 cm resolution in each horizontal

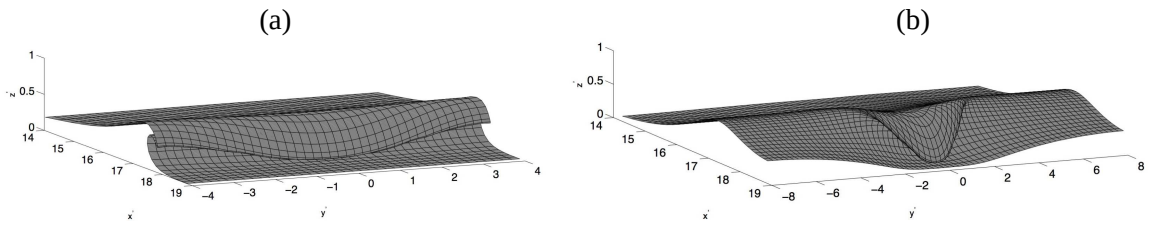

Figure 2: Examples of 3D overturning of a solitary wave over a sloping 1/15 ridge (with lateral sech^2 modulation), computed in the 3D-FNPF-NWT [45, 69]: (a) wide ridge; (b) narrow ridge.

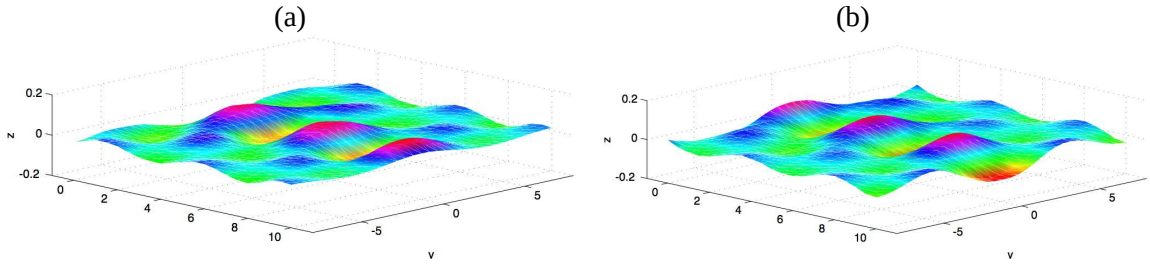

Figure 3: Examples of focused periodic waves computed in a 3D-FNPF-NWT by directional focusing, using a snake flap wavemaker [7, 8]: (a) and (b) show waves half a period apart.

direction, and similarly in the vertical direction (depending on depth). Considering the size of a typical large scale laboratory facility (e.g., order 50 by 50 by 2-3 m), such a resolution yields quite formidable numerical grids when using standard numerical methods (this aspect is detailed later).

Navier-Stokes (NS) equations for a Newtonian fluid, together with relevant free surface, bottom, and lateral boundary conditions, adequately model all the physics necessary to simulate complex wave and wave-structure interaction processes, including breaking. While great improvements have recently been made in 3D-NS models of complex wave processes (e.g., [1, 2, 4, 43, 80, 83]), their application over large computational domains (such as needed for representing a large 3D laboratory wavetank at proper spatial resolution) is still computationally prohibitive. More importantly, even if sufficient computer power were available, the excessive numerical diffusion of most current algorithms used, in fact makes NS models less accurate than inviscid wave models–such as based on Fully Nonlinear Potential Flow (FNPF) theory, discussed below–for simulating the essentially inviscid long range (or far field) wave propagation part of the computations [4, 46, 72]. Indeed, considering the negligible viscous effects in the core of the wave flow and the slow diffusion of vorticity from boundaries, until a breaker jet impacts the free surface, Kelvin theorem implies that initially irrotational waves, or flows starting from a state of rest (such as during generation by a wavemaker), will remain irrotational. Hence, prior to breaking, the irrotational solution of Euler equations, such as modeled in FNPF theory, is nearly exact. This is particularly true for the shorter distances of propagation in a physical wavetank, as evidenced by numerous comparisons of two-dimensional (2D) FNPF results with experimental measurements in precision wavetanks (e.g., for deep water plunging breakers [24, 90], or for shoaling and overturning waves over plane slopes [56, 58]). In the latter work, a 2D-FNPF model was found to predict the height and kinematics of shoaling solitary waves over mild slopes, within 2% of experimental measurements, up to the breaking point. Other 2D comparisons showed that the shape of such overturning waves is also accurately modeled up to touch down of a breaker jet [46, 59]. Upon impact of a breaker jet, strong vorticity and energy dissipation eventually occur, and a full Navier-Stokes (NS) model must be used together with a proper representation of the turbulence, as discussed above. For instance, NS models with Large Eddy Simulation (LES) of the 3D turbulent fields were successfully used to simulate 2D [12, 13, 80] and 3D [83] breaking and post-breaking solitary waves.

Therefore, the state-of-the-art in modeling strongly nonlinear surface wave generation, propa-

gation, and interactions with a complex bottom, up to breaking, is to apply FNPF theory in some way or form (see [22] for a review). [Note, that the long wave Boussinesq approximation (BM) of FNPF equations (standard or higher-order [102]) has proven successful for modeling long-wave propagation over a mildly sloping bottom, in the absence of steep submerged, surface-piercing, or floating structures. In addition to the latter limitations, BMs cannot really model wave generation by wavemakers and break-down when waves approach breaking.] With FNPF models, by contrast, various wave generation methods have been used and, when required, local dissipation or wave absorption has been simulated in an *ad hoc* manner (e.g., [49]).

For space-periodic problems over constant depth, with single-valued free surface elevation, very accurate and efficient solutions of FNPF equations have been proposed, based on the Higher-Order Spectral method or other similar unsteady Fourier theories (e.g., [6, 14, 23, 25, 38]). For non-periodic problems and/or complex bottom geometry, FNPF equations have typically been solved using a Boundary Integral Equation (BIE) method. Many such solutions have been proposed for 2D problems since the late 1970s, with the aim of studying overturning waves and other strongly nonlinear wave processes, first in deep then in shallow water (e.g., [16, 82, 84, 98]). Grilli and co-workers were among the first to develop efficient and accurate 2D-FNPF models directly in a *physical space region*, in which the BIE was solved based on a free space Green's function, using a higher-order Boundary Element Method (BEM). Incident waves were generated at one extremity and reflected, absorbed or radiated at the other extremity (e.g., [46, 49, 50, 53, 55, 56, 58, 59]). For these reasons, this group was also perhaps the first to have referred to such a model as a NWT [52]. [A more complete literature review can be found in some of the listed papers.] A comparatively smaller number of works have reported 3D-FNPF simulation, likely because of the more complicated geometric representation and intense computational effort. Single-valued 3D waves were simulated in arbitrary geometry, based on a BIE representation (e.g., [5, 11, 31, 88]), and 3D overturning waves were calculated in a doubly periodic domain with infinite depth [103, 104]. The latter authors analyzed the kinematics of plunging waves and quantified 3D effects on the flow. Only a few works to date have modeled 3D overturning waves in non-periodic domains, with bottom obstacles [9, 10].

Similar to their earlier 2D work, Grilli and co-workers developed an accurate 3D-NWT model [33, 47, 70] for strongly nonlinear wave generation, propagation over complex bottom topography, and interaction with obstacles. This model is based on a mixed Eulerian-Lagrangian [82] scheme, with explicit time stepping, and a spatial solution with a third-order BEM ensuring local continuity of the inter-element slopes. Arbitrary waves can be generated in this NWT, directly on the free surface or using snake wavemakers and, if needed, absorbing conditions can be specified on lateral boundaries. The higher-order representation and resulting high accuracy of this model's algorithms make it particularly well suited for simulating strongly nonlinear wave processes, extreme waves, and 3D wave overturning [7, 8, 35, 47, 68, 69]. Wave generation by an underwater landslide [28–30, 60] (with experimental validation), or by a moving surface pressure disturbance [91, 92] have also been simulated with this model. A full description of equations and numerical methods for this model can be found in references [45, 47]. Fig. 2, for instance, shows 3D solitary waves overturning over a sloping ridge, with lateral sech^2 modulation, and Figs. 3, 4 show the propagation of periodic waves, directionally focused using a snake wavemaker. In Fig. 3, waves exit (i.e., are absorbed in) the NWT through the back end, thanks to an actively absorbing snake wavemaker boundary. In Fig. 4, due to more intense energy focusing, extreme ("freak") waves are created that overturn in the middle of the tank.

The main drawback of the standard solution of FNPF equations with a BIE is its computational complexity, which grows with the cube of the discretization size N or, at best, with N^2 for an optimized iterative solution such as GMRES [68,69,103,104]. This greatly penalizes the efficiency of computations with a 3D-FNPF NWT, even on a heavily parallel computer cluster. One can

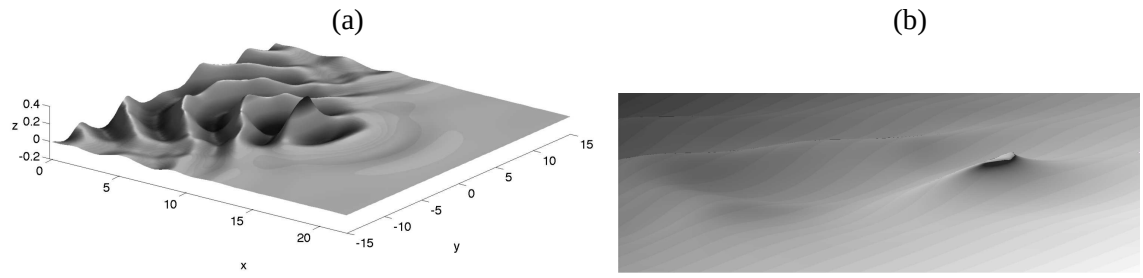

Figure 4: Examples of overturning extreme waves computed in a 3D-FNPF-NWT by directional focusing using a snake wavemaker [35, 45]: (a) View of the NWT free surface; (b) zoom on overturning wave crest.

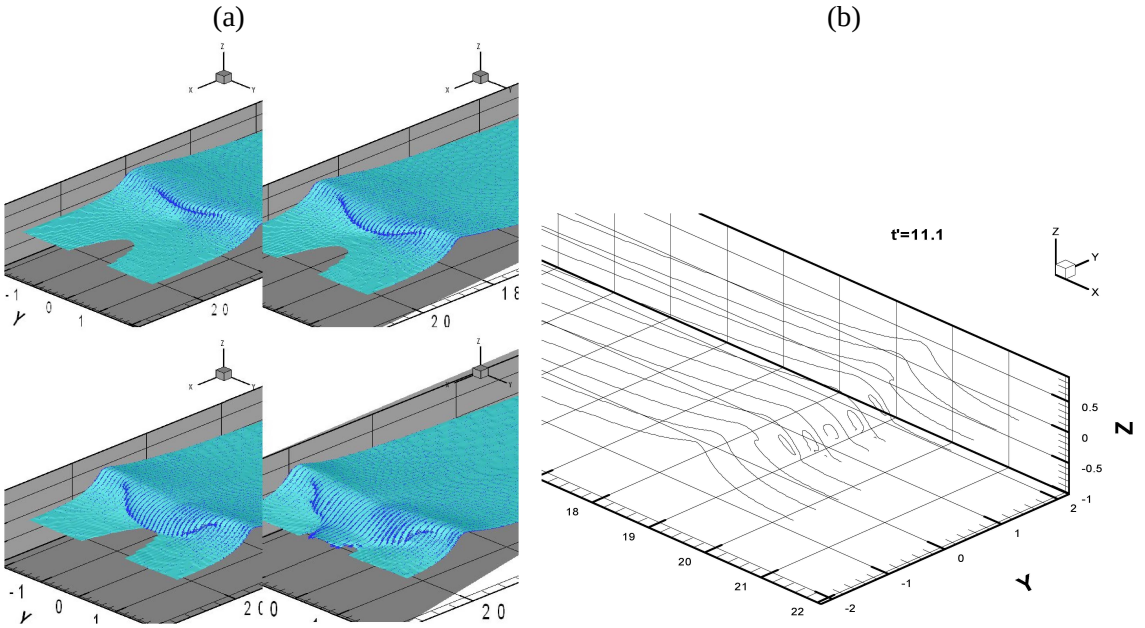

Figure 5: Modeling of a 3D solitary wave breaking over a sloping ridge (as in Fig. 2) in a *hybrid* 3D-FNPF-NWT/NS-VOF model [4]: (a) Phases of 3D breaking (b) 2D cross-sections.

greatly improve on this situation by implementing the Fast Multipole Algorithm (FMA; [41, 76, 86, 87, 89]). Using the FMA in the context of the present 3D-NWT, a $N \log N$ computational complexity, for $N > 4,000$, was achieving on a single processor machine [28, 29, 32, 34, 35, 45]. Recently, Grilli and co-workers implemented a version of this model for a large parallel cluster and were able to confirm the performance gain with the FMA up to 50,000 nodes, although only about 80% of each processor speed could be harnessed, in the best case scenario.

Note, the FMA numerical complexity is similar to that of the efficient Fast Fourier Transforms used, e.g., in HOS or other Fourier methods [6, 14, 23, 25, 38], although each computational step is typically more demanding in CPU time when using a BEM than in a HOS implementation.

3. NWT-NS MODEL COUPLING FOR WAVE-STRUCTURE-BOTTOM INTERACTIONS

FNPF theory is no longer applicable near an ocean or other rigid structure [105, 106], in the surfzone, or around steep bottom obstacles, when strongly nonlinear interactions takes place, causing local wave breaking and/or significant vortex shedding and viscous dissipation (e.g., vertical circular pile, rubble mound breakwaters, floating bodies with sharp edges, partially buried bottom obstacles, ...). Another model solving full NS equations, with a relevant turbulence closure

scheme, or a discrete particle model, must be applied near such structures [20, 26, 107]. As discussed above, however, full NS modeling can only be realistically performed in the "near-field", to achieve sufficient resolution and accuracy of the solution. In such cases, due to the computational expense, the NS computational domain surrounding the structure can typically only span a small number of significant dimension of the structure in each direction. Boundary conditions are usually provided to the NS model from another, simpler, wave model or theory based on potential flow equations, or an approximation or a variation of these. This approach, while accurate in principle, requires modeling the total flow in the NS model, i.e., incident waves plus perturbation caused by the structure, and to start computations from a state of rest. Both of these features make it difficult (or inaccurate) to express the radiation condition for the perturbation flow caused by the structure, at only a short distance away from it, and hence the size of the NS domain must be large enough. Additionally, NS computations will be quite demanding, since they must always be started from a state of rest. Another approach is to explicitly express the perturbation caused by the structure, bottom, or beach onto the otherwise nearly inviscid, irrotational wave flow.

3.1 Weak NWT-NS hybrid model coupling

Since the late 1990s, Grilli and co-workers pioneered a variety of model coupling, a.k.a. *hybrid modeling* strategies, to achieve a better efficiency and accuracy (since finer grids can be used) in such computations. Such coupled models combined FNPF modeling of wave propagation and/or shoaling (up to overturning) phases, to a NS modeling of the surfzone (for wave breaking on a slope or beach) or wave-structure interactions [4, 17, 46, 65, 77]. Fig. 5, for instance, shows simulations of 3D solitary waves breaking over a sloping ridge, similar to the case shown in Fig. 2, in a 3D-NS model, with a Volume of Fluid (VOF) representation of interfaces, initialized with results of a 3D-FNPF model [4]. Fig. 6, similarly shows computations of interactions of an extreme focused periodic wave, similar to the cases of Figs. 3, 4, with a circular pile, in a 3D-NS VOF model. In this case, the NS model is both initialized and has boundary conditions specified from results of the 3D-FNPF model.

Such cases are referred to as *weakly coupled models*, since no perturbation of the incident wave field is included due to the presence of the structure and the NS model is just initialized by the FNPF-NWT. The following section described a more recent FNPF-NS *strong model coupling* approach, which is more accurate in this respect.

3.2 Strong NWT-NS hybrid model coupling

To more accurately and efficiently simulate strongly nonlinear wave interactions with ocean structures or a beach, the 3D-FNPF-NWT and NS sub-models can be implemented concurrently in overlapping domains. This allows formulating governing equations for these models in a *strongly coupled* formalism. In this approach, the FNPF domain geometry encompasses the entire NWT (e.g., representing a large laboratory facility), featuring wave generation (e.g., by a snake wavemaker, a landslide,...) and wave energy dissipation on a sloping beach (through numerical absorption). The NS domain encompasses a smaller "near-field" region surrounding an ocean structure, the upper beach, or sediment and an obstacle on the ocean bottom . The wave fields, calculated in the FNPF model, are used to force computations in the NS model. In this methodology, pioneered by a few authors [3, 75], the total flow velocity and pressure are expressed as the sum of an irrotational "wave" component, satisfying FNPF equations, and a viscous perturbation. which . With this definition, NS equations are expressed for the *perturbation fields* only and the incident wave fields yield forcing terms for these equations. While this methodology has been proposed by others in this form, in earlier work, Grilli and co-workers implemented a similar approach to simulate wave-induced flow and sediment transport around solid objects on, or partially buried in, the seabed (Fig. 7a) [42,43]. In this case, a 3D-NS-LES model computational domain was entirely

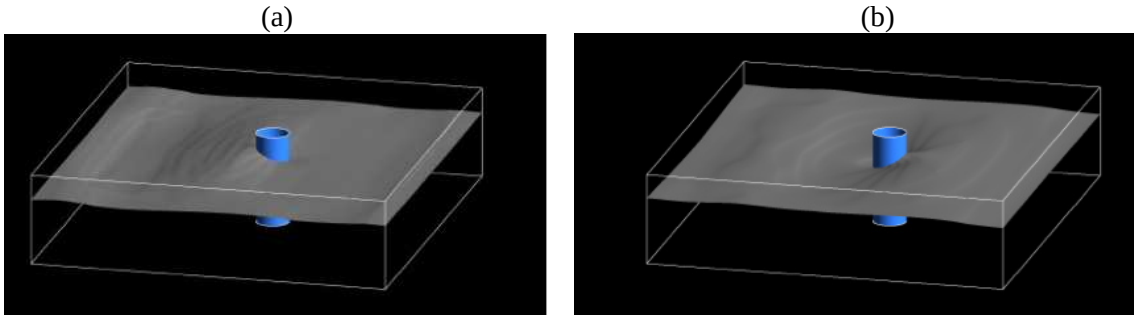

Figure 6: Modeling of the interactions of a 3D focused extreme wave and a vertical cylinder in a *hybrid* 3D-FNPF-NWT and 3D-NS VOF model [17]: (a) and (b), two phases of wave action.

submerged with a NWT in which far-field wave propagation and transformation were computed, and the dynamic wave pressure gradient calculated in the NWT was included as a source term in the 3D-NS model momentum equations.

In recent work [48], the same problem was re-implemented and solved following the more rigorous NS-perturbation field approach mentioned above. In doing so, the entire hybrid model, both FNPF-NWT and 3D-NS-LES were implemented and optimized for parallel processing on large computer clusters. Governing equations for the coupled-perturbed NS-LES model are given in the following.

Let us define the dynamic pressure $\hat{p}$ and total velocity V_i as a mean plus viscous/turbulent fluctuations,

$$\hat{p} = p + \rho g x_3 \qquad ; \qquad V_i = U_i + u_i \tag{1}$$

The time-averaged NS equations for an incompressible isothermal Newtonian fluid thus read,

$$\frac{\partial U_i}{\partial x_i} = 0 \qquad \text{and} \qquad \frac{\partial U_i}{\partial t} + U_j \frac{\partial U_i}{\partial x_j} = -\frac{1}{\rho}\frac{\partial \hat{p}}{\partial x_i} + \nu \frac{\partial^2 U_i}{\partial x_j \, \partial x_j} - \frac{\partial \overline{u_i u_j}}{\partial x_j} \tag{2}$$

with overbars indicating time-averages and the Reynolds stress tensor being defined as the sum of an isotropic and deviatoric part,

$$\overline{u_i u_j} = \frac{2}{3} k \, \delta_{ij} - T_{ij} \qquad \text{hence} \qquad -\frac{\partial \overline{u_i u_j}}{\partial x_j} = -\frac{2}{3}\frac{\partial k}{\partial x_i} + \frac{\partial T_{ij}}{\partial x_j} \tag{3}$$

with $k = \overline{u_k u_k}/2$ the turbulent kinetic energy. Defining the dynamic turbulent pressure as $\tilde{p} = \hat{p} - \frac{2}{3}\rho k$, and using first Eq. (2) and Eq. (3), second Eq. (2) transforms to,

$$\frac{\partial U_i}{\partial t} + U_j \frac{\partial U_i}{\partial x_j} = -\frac{1}{\rho}\frac{\partial \tilde{p}}{\partial x_i} + \nu \frac{\partial^2 U_i}{\partial x_j \, \partial x_j} + \frac{\partial T_{ij}}{\partial x_j} \tag{4}$$

For turbulence closure, we use a LES model [18, 108]. Accordingly, the deviatoric Reynolds stress tensor is expressed as,

$$T_{ij} = 2\nu_T S_{ij} - C_r L_{ij}^m \qquad \text{and} \qquad S_{ij} = \frac{1}{2}\left(\frac{\partial U_i}{\partial x_j} + \frac{\partial U_j}{\partial x_i}\right) \tag{5}$$

in which ν_T is a space varying eddy viscosity, whose parametrization is indicated below, L_{ij}^m is a tensor describing sub-grid scale turbulence, and S_{ij} is the resolved strain rate tensor. In Eq. (5),

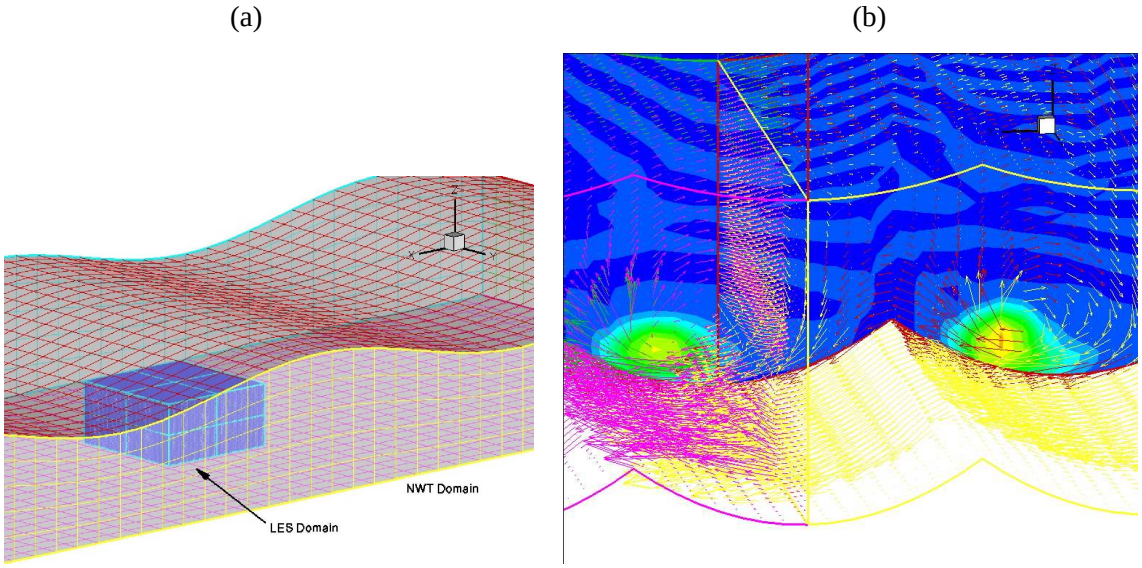

Figure 7: Strongly coupled 3D-FNPF-NWT/NS LES *hybrid* model, for near-bed wave-induced sediment transport [48]: (a) Sketch of model coupling; (b) Typical NS-LES velocity field (vectors) and suspended sediment concentration (contours) for a wave-induced oscillatory boundary layer, over parabolic vortex ripples.

C_r is either 0 or 1, depending on what type of turbulence closure scheme is used. Using Eq. (5), Eq. (4) becomes,

$$\frac{\partial U_i}{\partial t} + U_j \frac{\partial U_i}{\partial x_j} = -\frac{1}{\rho}\frac{\partial \tilde{p}}{\partial x_i} + (\nu + \nu_T)\frac{\partial^2 U_i}{\partial x_j \partial x_j} + \frac{\partial \nu_T}{\partial x_j}\left(\frac{\partial U_i}{\partial x_j} + \frac{\partial U_j}{\partial x_i}\right) - C_r \frac{\partial L_{ij}^m}{\partial x_j} \tag{6}$$

For convenience of the model discretization, we can recast Eq. (6) in the form,

$$\frac{\partial U_i}{\partial t} + \frac{\partial F_{ij}}{\partial x_j} = S_i \tag{7}$$

with, using Eq. (3),

$$F_{ij} = U_i U_j + \frac{\tilde{p}}{\rho}\delta_{ij} - (\nu + \nu_T)\frac{\partial U_i}{\partial x_j} \qquad \text{with} \qquad S_i = \frac{\partial \nu_T}{\partial x_j}\frac{\partial U_j}{\partial x_i} - C_r \frac{\partial L_{ij}^m}{\partial x_j} \tag{8}$$

For a Smagorinsky model, as used earlier [43], we set $C_r = 0$ and further define the eddy viscosity as, $\nu_T = C\Delta^2 |S_{ij}|$, where C is a problem dependent coefficient and Δ is a grid-filter width (typically, $\Delta = (\Delta x_1\, \Delta x_2\, \Delta x_3)^{1/3}$ where Δx_1, Δx_2, and Δx_3 denote characteristic grid length scales along each axis).

Let us now mark with superscript I the incident wave fields, described by an irrotational flow velocity, ($U_i^I = \nabla_i \phi^I, \tilde{p}_I = \hat{p}_I$, see next section for details) satisfying Euler equations,

$$\frac{\partial U_i^I}{\partial t} + U_j^I \frac{\partial U_i^I}{\partial x_j} = -\frac{1}{\rho}\frac{\partial \hat{p}_I}{\partial x_i} \qquad \text{with} \qquad \frac{\partial U_i^I}{\partial x_i} = 0 \tag{9}$$

and let us define the total mean flow as the sum of flow I and the (rotational and viscous) perturbation flow P, such that,

$$U_i = U_i^I + U_i^P \qquad \text{with} \qquad \tilde{p} = \tilde{p}^I + \tilde{p}^P \tag{10}$$

Replacing Eqs. (10) into first Eq. (2) and Eq. (6), and using Eqs. (9) yields,

$$\frac{\partial U_i^P}{\partial x_i} = 0 \tag{11}$$

$$\frac{\partial U_i^P}{\partial t} + \left(U_j^I + U_j^P - \frac{\partial \nu_T}{\partial x_j} \right) \frac{\partial U_i^P}{\partial x_j} + \frac{1}{\rho} \frac{\partial \tilde{p}^P}{\partial x_i} = -U_j^P \frac{\partial U_i^I}{\partial x_j} + (\nu + \nu_T) \frac{\partial^2 U_i^P}{\partial x_j \, \partial x_j} + \frac{\partial \nu_T}{\partial x_j} \left(\frac{\partial U_j^I}{\partial x_i} + \frac{\partial U_j^P}{\partial x_i} + \frac{\partial U_i^I}{\partial x_j} \right) \tag{12}$$

since irrotationality implies $\frac{\partial^2 U_i^I}{\partial x_j \, \partial x_j} = 0$.

We see, in addition to the viscous and turbulent terms in the right hand side of Eq. (12), there is a convection-like interaction term between the incident and perturbation velocity fields. The latter two equations are of the same form as first Eq. (2) and Eq. (6), but for the perturbation flow P, with the addition of forcing terms, which are functions of the incident wave fields I, obtained from the 3D-FNPF NWT "far field" solution. With a BIE/BEM method, this solution is expressed both directly on the boundary and, through explicit integration, for any interior point as a function of the boundary solution [47, 69]. Such interior points can be defined as coordinates of the NS-LES model discretization cell centers, and thus be calculated as time series of velocity U_i^I and velocity gradient $(\frac{\partial U_j^I}{\partial x_i}, \frac{\partial U_i^I}{\partial x_j})$ values.

The above was implemented for a NS-LES domain submerged within a NWT. Current results in addition assume that the incident wave field is mostly varying in a vertical plane, and hence is 2D, over the lateral scale of the NS domain, due to the latter small size as compared to typical scales of lateral wave variation. Hence, the 2D version of the FNPF-NWT [44, 49, 53, 55, 61, 62] was used to compute incident fields *I*, although there is no additional difficulty in principle (except for a heavier computational cost) to use the 3D version of the NWT [33, 45, 47, 70], with FMA implementation [28,32,34,35,91,92]. Using a 2D-NWT in fact, has made it possible computing at moderate cost long term fully nonlinear irregular shoaling fields, to force the 3D-NS-LES model, such as based on a specified standard wave energy spectrum [39].

An additional difficulty occurs with this methodology, when there are surface piercing structures or a beach, with the possibility of wave breaking and dissipation occurring at the free surface, thus requiring the NS domain to also be surface piercing. Hence, a similar decomposition into incident and perturbation fields must be done for the kinematic and dynamic free surface boundary conditions in the NS model (as, e.g., done in [3] for floating bodies in waves), which, due to nonlinearity, yields new interaction terms between the I and P fields. The difficulty then resides in expressing the *I* forcing fields at the location of the total fields, which in some case may be outside of the NWT domain (see, e.g., Alessandrini [3] for details, and the application of the method when using a HOS model to compute the *I* fields). Note, however, that the presence of fixed (rigid or flexible) or floating structures [105, 106] in the NS domain only affects the computation of the perturbation fields and thus is easily included in this coupling method. The no-flow condition on a fixed rigid structure in the NS model, for instance reads $U_i^P n_i = -U_i^I n_i = -\frac{\partial \phi^I}{\partial n}$, with n_i the normal vector.

Thus, in the proposed approach, the same numerical model (here solving complete 3D-NS-LES equations) is used to solve for the perturbation fields P only; as indicated, wave forcing terms in the modified NS discretized equations are provided from the NWT. One important feature, though, as indicated above, is that the perturbation flow decays away from the source of perturbation, i.e., the ocean structure, bottom, or the surfzone. Hence, boundary conditions for the P fields, on the "near-field" NS-LES computational domain boundary (e.g., Fig. 7a) become radiation conditions : $U_i^P \rightarrow 0$, and $\tilde{p}^P \rightarrow 0$. These, practically, can be modeled as a *sponge layer*, in which the

perturbation fields gradually decay and vanish on the boundary. Since forcing from the incident wave fields I is included as volume terms in NS equations, there is no need for additional boundary conditions. Figure 7b shows an example of results obtained in a strongly coupled NWT-NS *hybrid* model, for wave-induced flow (and sediment suspension) above sand bottom ripples [48].

Finally note that this coupling method is *exact* for the NS equations, even though it may not appear so at first glance. The only approximation made here is to describe the incident wave fields as irrotational outside of the NS computational domain (and hence dynamically inviscid).

3.3 Equations and boundary conditions for NWTs

Governing equations for a 2D- or 3D-FNPF-NWT are briefly presented in the following (see 2D [44, 49, 53, 55, 61], 3D [33, 45, 47], for details). The velocity potential for far-field, irrotational waves, $\phi^I(x_i, t)$ is introduced in the vertical plane (x, z) (2D) or in space (x, y, z) (3D) and the corresponding velocity is defined by, $U_i^I = \nabla_i \phi^I \equiv (u, (v), w)$. Mass conservation/continuity equation in the fluid domain $\Omega(t)$ with boundary $\Gamma(t)$ is a Laplace's equation for the potential (Fig. 1; Fig. 7a),

$$\nabla_j(\nabla_j \phi^I) \equiv \nabla^2 \phi^I = 0 \qquad \text{in } \Omega(t) \tag{13}$$

Using Green's 2nd identity, Eq. (13) is transformed into a Boundary Integral Equation (BIE; bold symbols now indicate vectors),

$$\alpha(\boldsymbol{x}_l)\, \phi^I(\boldsymbol{x}_l) = \int_\Gamma \left\{ \frac{\partial \phi^I}{\partial n}\, G - \phi^I\, \frac{\partial G}{\partial n} \right\} d\Gamma \tag{14}$$

where the Green's functions are defined as,

$$\begin{aligned} G(\boldsymbol{x}, \boldsymbol{x}_l) &= -\frac{1}{2\pi} \log r \quad \text{or} \quad \frac{1}{4\pi r} \\ \frac{\partial G}{\partial n} &= -\frac{r_j n_j}{2\pi\, r^2} \quad \text{or} \quad -\frac{r_j n_j}{4\pi\, r^3} \end{aligned} \tag{15}$$

for 2D or 3D problems, respectively, with $r_i = x_i - x_{li}$, $r = \mid \boldsymbol{r} \mid$, $\boldsymbol{x} = (x, (y), z)$ and $\boldsymbol{x}_l = (x_l, (y_l), z_l)$ position vectors for points on the boundary, $\boldsymbol{n} = (n_x, (n_y), n_z)$ the outward unit normal vector to the boundary, and $\alpha(\boldsymbol{x}_l)$ is a geometric coefficient function of the exterior angle of the boundary at $\boldsymbol{x}_l$ (usually $\simeq 1/2$ for a smooth boundary geometry).

Boundary Conditions: On the free surface Γ_f, ϕ^I satisfies the kinematic and dynamic boundary conditions,

$$\frac{D\, R_i}{D\, t} = (\frac{\partial}{\partial t} + U_j^I \nabla_j)\, R_i = U_i^I = \nabla_i \phi^I \qquad \text{on } \Gamma_f(t) \tag{16}$$

$$\frac{D\phi^I}{Dt} = -gz + \frac{1}{2} \nabla_j \phi^I \nabla_j \phi^I - \frac{p^I{}_f}{\rho} \qquad \text{on } \Gamma_f(t) \tag{17}$$

respectively, with R_i, the position vector on the free surface, g the gravitational acceleration, z the vertical coordinate, p_f^I the free surface pressure, and ρ the water density. Along the bottom boundary Γ_b, a no-flow condition is prescribed as,

$$\overline{\frac{\partial \phi^I}{\partial n}} = 0 \qquad \text{on } \Gamma_b \tag{18}$$

where the overline denotes specified values.

From Bernoulli Eq. (17), the wave-induced dynamic pressure within Ω, is expressed as,

$$\hat{p}^I = p_f^I - \rho \left\{ \frac{\partial \phi^I}{\partial t} + \frac{1}{2} U_j^I U_j^I \right\} \tag{19}$$

The computation of the internal solution based on the boundary solution is explicit in the BEM. Details are given in a section below.

Wave generation: Various methods have been used for wave generation in this NWT [7, 8, 35, 44, 49, 55, 60]. In applications reported here, similar to laboratory wavetank generation of deep or shallow water periodic or random waves [39, 42, 43, 46, 56, 61, 62], waves are generated on boundary Γ_w using a rigid wavemaker (piston or flap type) moving according to a prescribed stroke, $x_w = S(t)$ at height y_w. For a simple piston wavemaker, for instance, we have,

$$\overline{\frac{\partial \phi^I}{\partial n}} = -\frac{\mathrm{d}\, x_w}{\mathrm{d}\, t} \qquad \text{on } \Gamma_w \tag{20}$$

where the time derivative follows the wavemaker motion. Wavemaker laws for this and other more complex wavemaker types can be found in references. [Note, the wavemaker motion is usually ramped-up over two or three representative wave periods, by modulating the stroke with a tanh function of time. See references for details.]

Wave absorption: During shoaling of a periodic wave over a slope and prior to breaking (which, on a mild slope, approximately occurs when the ratio of wave height over depth $\kappa = H/h \simeq 0.8$), wave steepness and asymmetry (both between trough and crest and between front and rear of each wave; e.g., Fig. 1) continuously increase. The present work focuses on the viscous flow near the bottom or around structures induced by such highly nonlinear and asymmetric waves, prior to breaking. Breaking is prevented in the NWT by dissipating incident wave energy in a numerical Absorbing Beach (AB), located beyond the area of interest (e.g., Fig. 1).

Following Grilli and Horrillo [49], in the absorbing beach (AB), specified for $x \geq x_a$, an external pressure $p_f^I = p_a$ is applied to the free surface, by way of the dynamic boundary condition (17) (with $z = \eta$), to create a negative work and absorb wave energy. Typically, additional amplitude reduction is induced by causing de-shoaling in the AB, by specifying a bottom geometry somewhat similar to that of a natural bar (e.g., with a depth increasing from $h(x_r)$ to h_1). The AB "absorbing pressure" is specified proportional to the normal particle velocity on the free surface (in 2D- or 3D-NWT),

$$p_a(x, (y), \eta, t) = \nu_a(x)\, \frac{\partial \phi^I}{\partial n}(\eta(x, (y), t)) \tag{21}$$

where ν_a is the AB absorption function defined as,

$$\nu_a(x) = \nu_{ao}\, \rho \sqrt{g h_1}\, f(x) \tag{22}$$

where ν_{ao} is a non-dimensional beach absorption coefficient, and $f(x)$ follows a $\tanh$ variation for $x_a \leq x \leq x_r$, and $f(x) = 1$ for $x_r < x \leq x_p$. first ramped-up from 0 to ν_{ao} and then maintained constant over the AB. More specifically,

An absorbing piston (AP; [15, 49]) is also specified at the extremity of the AB, for $x = x_p$. This AP moves proportionally to the hydrodynamic pressure force caused by waves, calculated as a function of time in the NWT (see references for details). For periodic waves, Grilli and Horrillo showed that the combination AB/AP effectively absorbs incident wave energy in the NWT, to within any specified small fraction. This was recently verified for irregular waves as well [39].

Bottom friction: For short distances of propagation over a smooth bottom, wave damping due to bottom friction is quite small, and is usually neglected in numerical models, even for long waves,

when the computational domain only spans a few wavelengths (e.g., [46, 56, 58, 59]). To simulate wave shoaling over a rippled sandy bed, which may induce more significant wave damping due to bed roughness, Grilli et al. [61, 62] simulated an energy dissipation term due to bottom friction in the NWT. They did so by specifying a surface pressure distribution, similar to that detailed above for the AB, over the shoaling region for $x_w < x \leq x_a$ (Fig. 1).

In the applications reported here, we did not assume a rough or moving sediment bed and, hence, neglected bottom friction effects on wave shape and velocities. Such effects could however be included if necessary.

Solution for Internal Fields: Internal velocity values, and their gradients, are required to force NS-LES model computation of the perturbed fields in real time (Eqs. (12)). and velocities, together with the time derivative of the potential, are needed to calculate the wave-induced internal dynamic pressure $\hat{p}^I$ (Eq. (19)).

At each time step, the NWT provides the solution for the velocity potential ϕ^I, its normal derivative, and the time derivative of these (due to the second-order time integration scheme used; see later) on boundary Γ. Potential ϕ^I, can then be explicitly calculated, for any point $\boldsymbol{x}_l$ within domain Ω, based on the boundary solution. This is done using the same BIE (14),(15), as solved on the boundary, but expressed for $\alpha_l = 1$ at an interior point. If we denote by ∇_{li} the gradient operator with respect to the coordinates of point $\boldsymbol{x}_l \in \Omega$, Eq. (14) yields,

$$\frac{\partial \phi^I}{\partial t}(\boldsymbol{x}_l) = \int_\Gamma \left\{ \frac{\partial^2 \phi^I}{\partial t \partial n} G - \frac{\partial \phi^I}{\partial t} \frac{\partial G}{\partial n} \right\} d\Gamma \tag{23}$$

and,

$$\boldsymbol{U_i^I}(\boldsymbol{x}_l) = \int_\Gamma \left\{ \frac{\partial \phi^I}{\partial n} (\nabla_{li} G) - \phi^I \left(\nabla_{li} \frac{\partial G}{\partial n} \right) \right\} d\Gamma \tag{24}$$

with, in 2D- and 3D-NWT,

$$\begin{aligned} \nabla_{li} G &= \frac{r_i}{2\pi\, r^2} \quad \text{or} \quad \frac{r_i}{4\pi r^3} \\ \nabla_{li}\left(\frac{\partial G}{\partial n}\right) &= \frac{1}{2\pi\, r^2}\left\{ n_i - 2 r_i \frac{r_j n_j}{r^2} \right\} \quad \text{or} \quad \frac{1}{4\pi\, r^3}\left\{ n_i - 3 r_i \frac{r_j n_j}{r^2} \right\} \end{aligned} \tag{25}$$

[Note, derivatives with respect to internal point coordinates have been directly applied to the Green's functions in the integrand in Eq. (24).] Internal velocity gradients, which are forcing terms in Eq. (12), are similarly obtained by applying ∇_{lj} to Eq. (24). See detailed 2D and 3D expressions in references [43, 69].

3.4 Non-cohesive Sediment Transport Model

In work in progress, the strongly coupled hybrid model (2D-NWT and 3D-NS-LES) is used to simulate non-cohesive sediment transport and resulting scouring around a partially buried rigid object on the bottom, induced by fully nonlinear irregular and shoaling waves [39, 42, 43, 48] (Figs. 1, 7). Thus, suspended sediment concentration is modeled with a volume-filtered advection-diffusion equation,

$$\frac{\partial \overline{C}}{\partial t} + \frac{\partial}{\partial x_j}\left((U_j^I + U_j^P - w_s \delta_{i2}) \overline{C} + \overline{u_j C} \right) = 0 \tag{26}$$

where C is sediment concentration by volume fraction, and w_s is sediment fall velocity (function of sediment properties, size and shape). Consistent with the common assumption in the literature that the turbulent Schmidt number $\sigma = 1$, the same Smagorinsky subgrid-scale turbulence model

is adopted for the fluctuation terms in both the momentum and this sediment concentration ($\overline{u_j C}$) equations.

Boundary Conditions: For the inflow/outflow and top boundaries of the NS-LES domain (Γ_i, Γ_o, Γ_t), we have used gradient free boundary conditions (Fig. 7a).

For the bottom boundary Γ_b, an empirical function developed by van Rijn [96] is used for evaluating the sediment concentration near the bed, as it varies along the bed,

$$C_a = 0.015\,\frac{d_{50}}{k_s}\,\frac{T^{1.5}}{D_*^{0.3}} \quad \text{with} \quad T = \frac{u_*^2 - u_{*,\mathrm{CR}}^2}{u_{*,CR}^2} \quad \text{and} \quad D_* = d_{50}\,\frac{\left((s-1)\,g\right)^{1/3}}{\nu^2} \tag{27}$$

where d_{50} denotes the median grain equivalent diameter of the sediment of dry specific density $s = \rho_s/\rho_w$, the bottom shear velocity is u_*, the critical shear velocity is $u_{*,\mathrm{CR}}$ (obtained from a critical Shields parameter curve as a function of D_*; e.g., Eq. 4.1.1 in [97]), and the roughness height is k_s.

In order to compute u_*, we solve the boundary layer log (wall) law, $u/u_* = \frac{1}{\kappa}\log\left(y + y_0\right)/y_0$ (where, $\kappa \simeq 0.3$ is the Von Karman parameter, $y_0 = k_s/30$, and y here denoting the normal direction away from the boundary within the fluid), at each location along the bed, using as inputs the velocity computed from the previous time step at the grid point nearest to the bed location and the distance of that point to the bed. Nakayama et al. [85] showed that, for *smooth wall* flows, the filtered (in the LES sense) instantaneous wall shear stress and velocity at points above the bed correlate well, and hence a log-law relationship is reasonable. Nakayama (personal communication, 2005) further indicated that the relationship holds as well for *rough walls* and our recent simulations (reported below) seem to confirm this statement, by comparing well with laboratory experiments. Additional justifications and discussions regarding the use and relevance of Eqs. (27) can be found in references [43, 48].

3.5 Summary of Numerical Methods used in Hybrid Models

3.5.1 Numerical Wave Tank

In 2D- and 3D-NWTs, the BIE (14) is solved by a Boundary Element Method (BEM), by expressing it for N discretization nodes on the boundary $(\boldsymbol{x}_l; l = 1\ldots, N)$, and defining M higher-order elements to interpolate in between discretization nodes. In the present 2D applications, quadratic isoparametric elements are used on lateral and bottom boundaries, and cubic elements ensuring continuity of the boundary slope are used on the free surface. In these elements, referred to as Mid Cubic Interpolation (MII) elements, both geometry and field variables are interpolated between each pair of nodes, using the mid-section of a four-node "sliding" isoparametric element [55]. The Green's function and its normal derivative in Eq. (15) are singular as $r \to 0$. These singularities require additional treatments whose detailed derivations will not be included here. These can be found in [44, 53, 55], for both 2D isoparametric and MII elements; 3D BEM and integrations used in the 3D-NWT can be found in [45, 47], with the FMA implementation in [34]. Note, a recent implementation of accelerated local Green's function for the 2D-NWT is presented in [39]. It should be noted that, when applying Eq. (14) to points $\boldsymbol{x}_l$ that are very close to a different part of the boundary (e.g., near corners in Fig. 1), almost-singular integrals will occur when r is very small. The numerical accuracy of such integrals is improved by applying an adaptive integration method [54, 55, 57].

Time integration: Free surface boundary conditions (16) and (17) are time integrated based on two second-order Taylor series expansions expressed in terms of a time step Δt and of the

Lagrangian time derivative, D/Dt, for R_i and ϕ^I,

$$\begin{aligned}
\overline{R_i}(t+\Delta t) &= R_i(t) + \Delta t \frac{D\,R_i}{D\,t}(t) + \frac{(\Delta t)^2}{2}\frac{D^2 R_i}{Dt^2}(t) + \mathcal{O}[(\Delta t)^3] \\
\overline{\phi}^I(t+\Delta t) &= \phi^I(t) + \Delta t \frac{D\,\phi^I}{D\,t}(t) + \frac{(\Delta t)^2}{2}\frac{D^2 \phi^I}{Dt^2}(t) + \mathcal{O}[(\Delta t)^3]
\end{aligned} \tag{28}$$

respectively. First-order coefficients in the series correspond to free surface conditions (16) and (17), in which ϕ^I and $\partial\phi^I/\partial n$ are obtained from the BEM solution of the BIE (14) for (ϕ^I, $\partial\phi^I/\partial n$) at time t. Second-order coefficients are expressed as D/Dt of Eqs. (16) and (17), and are calculated using the solution of a second similar BIE for ($\partial\phi^I/\partial t$, $\partial^2\phi^I/\partial t\partial n$), for which boundary conditions are obtained from the solution of the first BIE and the time derivative of Eqs. (17) to (20). Detailed expressions of the Taylor series coefficients for the 2D-NWT can be found in [44, 53]; similar expressions for the 3D-NWT can be found in [33, 45, 47].

At each time step, the overall numerical accuracy is estimated by computing errors in volume and energy of the computational domain. Earlier work shows that, for both 2D and 3D problems, such errors are function of both the size (i.e., distance between nodes) and the degree (i.e., quadratic, cubic,...) of boundary elements used in the spatial discretization, and of the size of the selected time step [47, 55, 57]. Thus, the optimal time step, is adaptively selected based on a mesh Courant number, whose optimal value for 2D- or 3D-MII elements was shown to be about 0.45. This value is used in the present applications.

In long term computations involving finite amplitude waves, mean drift currents occur ("Stokes drift"), which continuously move free surface discretization nodes/Lagrangian markers away from the wavemaker into the NWT. Hence, when performing computations over many wave periods or long time series of irregular waves [39], nodes are redistributed (i.e., regridded at constant arclength intervals, or over a fixed horizontal grid, on selected sections of the free surface) after fixed numbers of time steps.

Solution for Internal Fields: All of the integrals in Eqs. (23) and (24) (and their additional derivative for velocity gradients) expressing interior fields are non-singular and can be evaluated by Gauss quadrature. However, for interior points located very close to boundary Γ, similarly to corner points in the original discretized BIE (14) (see, e.g., [57] in 2D and [47] in 3D), the integral kernels will rapidly grow as r becomes small, yielding inaccurate numerical integration over parts of the boundary nearest those points. This is even more so when the operator ∇_{li} has been applied to the Green's functions, as in Eqs. (25) (and its additional derivative for velocity gradients), where in 2D-NWT, terms are $O(1/r)$ to $O(1/r^3)$ for small r (and of even higher power in $1/r$ for the 3D-NWT). Grilli and Svendsen [57] and Grilli and Subramanya [54] studied these numerical integrations in detail, referred to as quasi-singular integrals (QSI). Following their method, in NWT computations, a geometrical analysis of the discretization is made at each time step, where QSIs are identified based on a distance criterion. During numerical integration of the various BIEs, both for the boundary solution and for internal points, QSIs are then integrated using an adaptive integration method, in which elements are subdivided into an increasingly large number of sub-segments, as a function of a distance-based algorithm. The originally selected number of Gauss points is used within each sub-segment. Grilli and Subramanya [54] showed that, given enough sub-segments, this method can provide almost arbitrary numerical accuracy of the QSIs. A similar method was implemented in the 3D-NWT [47].

3.5.2 Navier-Stokes Model

The scheme referred to as QUICK [78] is used for the spatial discretization of the advection terms in the 3D momentum Eqs. (12), and central differences for all other terms. The same methods are used for discretizing the advection-diffusion Eq. (26) for the sediment concentration

field, except that SHARP [79] is used in place of QUICK, owing to its improved handling of sharp gradients. Both equations employ a Crank-Nicolson averaging for the diagonal viscous terms, and the Adams-Bashforth method for all other terms, which yields a semi-implicit, quasi-tridiagonal system of equations.

This system of equations is solved with a fractional step method. In this method, an estimate of the velocity field is first obtained by solving NS equations without the pressure term, the pressure Poisson equation is solved for the pressure as driven by the estimated velocity field, and the velocity estimate is corrected with the pressure to satisfy continuity.

Further details about the equations, discretization, and numerical methods can be found in Zang et al. [108, 109] and Tseng and Ferziger [95]. A discussion of recent improvements to some of the above algorithms as well as of the parallel implementation can be found in [48].

Immersed Boundary Method (IBM) : The IBM is used to specify the fluid bottom boundary condition in the NS-LES model, in case of a moving sediment bed, i.e., a few cells below seabed. Hence, the IBM works by applying the force necessary at the location of the immersed boundary, to enforce the physical boundary condition, $u_i = 0$ in this case. [The implementation of a log-law in the IBM over a complex boundary is difficult so, as an approximation, we assume that the boundary lies at the y_0, the location where the log-law velocity is zero.] Of the many versions of the code originally developed by Zang et al. [109], we employ the modified ghost cell method of Tseng and Ferziger [95].

Additionally, in recent developments [48], the friction velocity is determined locally based on the horizontal velocity at the first grid point above the wall (i.e., immersed boundary). The boundary has then a stress applied corresponding to the friction velocity More details can be found in references

4. APPLICATIONS

In addition to applications of the 2D- and 3D-NWTs already discussed, we present here recent simulations, in a 2D-NWT/3D-NS-LES hybrid model formulated for the *perturbation fields P*, as detailed earlier in this paper. These are cases of wave-induced flows near a smooth or a rough bottom, and sediment transport induced around a partly buried cylinder, which are either new simulations or repeats of simulations performed with the earlier version of the models, in which NWT/NS-LES model coupling was effected through the less rigorous pressure gradient term and the boundary layer wall function was more arbitrarily set [43]. The present models have also been fully parallelized and optimized for large computer clusters, which will make it possible simulating problems at very high resolution and over a long time in the near future. [Note, this work was performed by Grilli and co-workers Harris and Greene [48]. We run the model in its most recent MPI parallel implementation, on a 16 processor computer.]

The hybrid model set-up is such as shown on Fig. 7a. In these applications, the BEM NWT is 2D and discretized only on its boundary. Waves are generated at one extremity by a wavemaker and absorbed with an AB/AP at the other extremity (as in Fig. 1). The 2D wave flow fields are specified as forcing fields in the 3D-NS-LES model equations expressed for the P fields. The NS-LES model domain is discretized with regular meshes of size Δx, Δy, and Δz along each direction.

4.1 Oscillatory laminar boundary layer

This is a more academic application of the hybrid model, to an idealized problem (also know as Stokes problem), of an oscillatory flow over a smooth (infinite) solid plate, for which there is an analytic solution. The irrotational flow forcing the NS model, here, is simply a specified uniform harmonic current $U^I(y,t) = U_o \sin \omega t$, of period $T = 2\pi/\omega$, in the x direction, with y the vertical

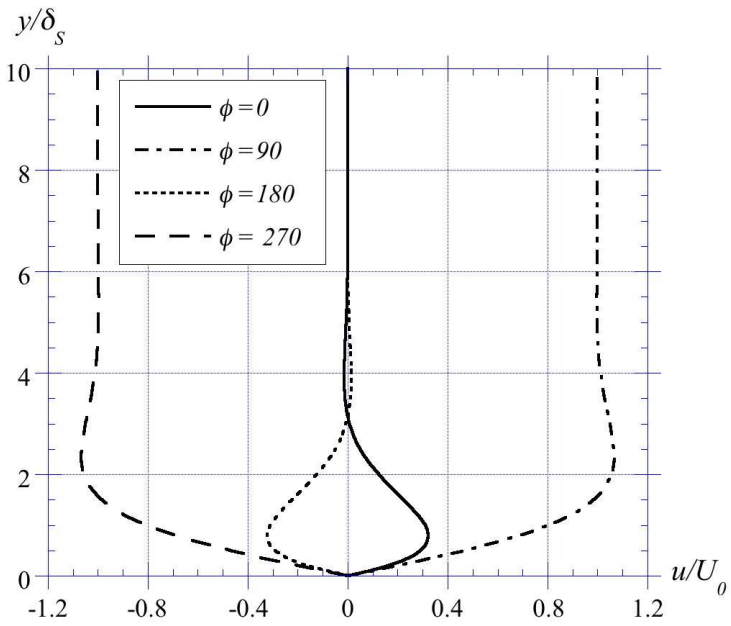

Figure 8: Stoke's analytical solution (Eq. (29)), for an oscillatory laminar boundary layer, as a function of phase angle $\phi = \omega t$.

direction; hence, in this problem, there is actually no need for computations in the NWT.

Spatial periodicity of the NS solution for the P fields is specified in the x and z directions. A no slip condition $u_i = 0$ is specified on the bottom boundary at $y = 0$, and the free stream velocity U^I is specified at $y = h$ above the plate, with $(v = w = 0; \partial u/\partial y = 0)$. For a low Reynolds number Re, the (mean=total) velocity $u(y) = U = U^I + U^P$ near the plate takes the form of a laminar boundary layer for which an analytical solution can be derived as,

$$u(y) = U_o \left\{ \sin \omega t - e^{-\frac{y}{\delta_S}} \sin\left(\omega t - \frac{y}{\delta_S}\right) \right\} \tag{29}$$

with $\delta_S = \sqrt{2\nu/\omega}$, the Stokes layer thickness. This solution applies for $Re = U_o \delta_S/\nu < 100$. Hence, by comparing the numerical and analytical solutions, both the NS model result accuracy and convergence rate can be assessed as a function of grid size and time step.

In the following, we set $Re = 1$, $\delta_S = 1$, $U_o = \pi$ and $\nu = \pi$. The NS domain dimensions are $h = 16\delta_S$ in each direction, and the spatial grids are identical in each direction as well (i.e., $\Delta x = \Delta y = \Delta z$). The model is ramped-up for $100T$ and maximum relative errors on flow velocity ε/U_o, are calculated at $t = 100T$. Figure 8 shows the analytic solutions (Eq. (29)) for 4 phase angles of the flow, $\phi = \omega t$ and Fig. 9 shows numerical errors when varying time step Δt for a fixed grid size ($\delta_S/64$), or varying the grid size for a fixed time step ($\Delta t = T/1000$). Errors reduce as expected when reducing either grid size or time step and closely follow (or outperform) the second-order convergence (expected from the model's discretization and time integration schemes) in the typical range of parameter values.

4.2 Oscillatory turbulent boundary layer

This problem is similar in set-up and flow forcing to the previous one, but now for an oscillatory flow with higher Reynolds number over a rough flat plate. This creates a turbulent oscillatory boundary layer flow structure, for which there is no longer an analytical solution. In this case, model results are compared to Jensen et al.'s [74] laboratory experiments, performed in an oscil-

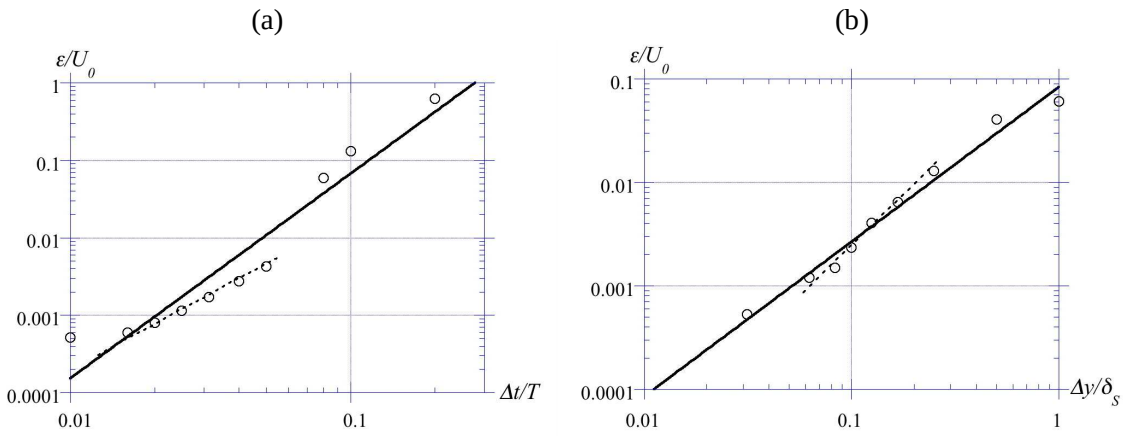

Figure 9: Relative numerical error of computed velocity, as compared to Eq. (29), for an oscillatory laminar boundary layer, as a function of: (a) time step, for $\Delta y = \delta_S/64$; (b) grid size for $\Delta t = T/1000$. (——) is a best power fit to the data and (- - - -) shows second-order convergence.

lating water tunnel (U-tube), with flows driven by a pressure gradient. The bed roughness was 0.35 mm in experiments (sand paper). For this case as well, there is no need for running the NWT, but results nevertheless allow to assess the accuracy of all the important features of the NS-LES model, i.e., regarding flow forcing, bottom boundary condition, and turbulence representation. The new parallel implementation is also being validated as well.

The NS-LES model set-up and boundary conditions are identical to the previous case, and physical parameters are selected to match experiments (case 13) with $U_o = 2$ m/s, $T = 9.72$ s, $\nu = 1.14\,10^{-6}$ m^2/s (i.e., $\delta_S = 1.9$ mm and $Re = 3,295$), and $u_* = 0.11$ m/s (as measured from the boundary layer structure near the bed). In the model, we specify a log-layer near the rough plate, with $z_o = k_s/30 = 0.028$ mm, which yields $u_* = 0.104$ m/s for the Smagorinsky scheme, thus in close match with experiments. The NS computational domain is 0.384 m long in the y direction and half that in each lateral direction; spatial discretization is constant in each direction as $\Delta x = \Delta y = \Delta z = 6$ mm and time step is $\Delta t = 0.001$ s. The NS-LES solution is ramped-up for $10T = 97.2$ s, and both mean and turbulent velocities are computed for $t = 10T$ and compared to experimental measurements.

Figure 10a first shows that the mean horizontal velocity predicted in the model ($u = U = U^I + U^P$) is in close agreement with experimental measurements at two phases of the flow. Fig. 10b then shows that the RMS of the horizontal turbulent velocity ($u' = u^P$) is in reasonable agreement with measurements at the same phases of the flow. This confirms the overall soundness of the NS-LES model in representing turbulent oscillatory boundary layers, such as typically induced by ocean waves near the rough seabed. The good agreement of turbulent flow features, in particular, is key to the correct modeling of the suspension and transport of fine non-cohesive (i.e., sandy) sediment. This is illustrated in the next application of the full hybrid model.

4.3 Wave-induced sediment transport around bottom obstacle due to periodic waves

In this application, the set-up is similar to that shown in Fig. 1, and also detailed in [43, 61, 62]. Waves are generated in the 2D-NWT and propagate over a small bottom obstacle (such as a small cylinder). The NS-LES model domain is a small box located around the obstacle and enclosing a small portion of the seabed with it (as sketched in Fig. 7a).

Although this aspect is not illustrated in the following application, the 2D-NWT was recently improved [39], both in efficiency for large discretization (through using a localized Green's func-

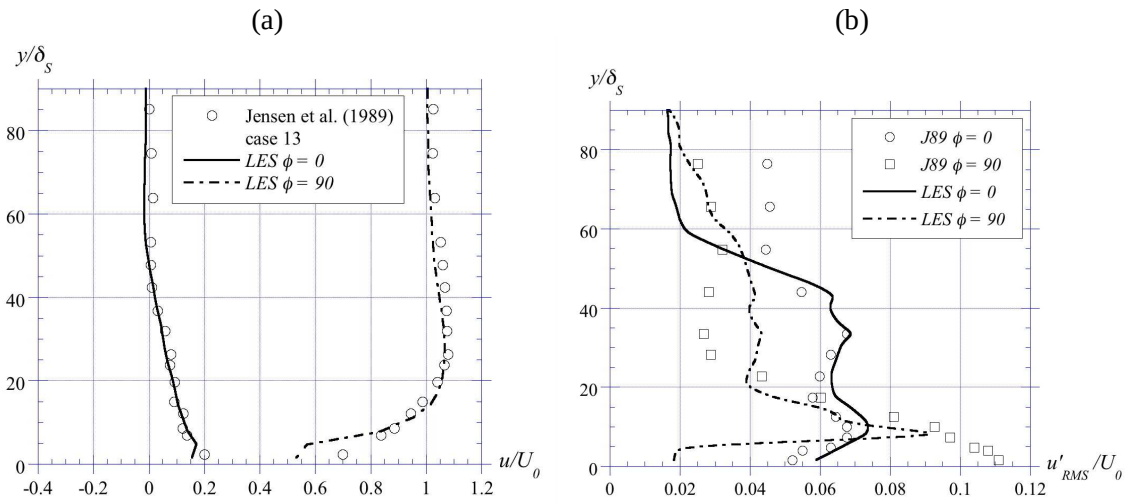

Figure 10: Comparison of horizontal velocity computed in NS-LES model (——) or (– - –), to experimental measurements (○) [74], for a rough turbulent oscillatory boundary layer: (a) mean velocity for two phase angles; (b) RMS of turbulent velocity for two phase angles ($U_o = 2$ m/s, $T = 9.72$ s, $\nu = 1.14\,10^{-6}$ m^2/s, $\delta_S = 1.9$ mm and $Re = 3,295$).

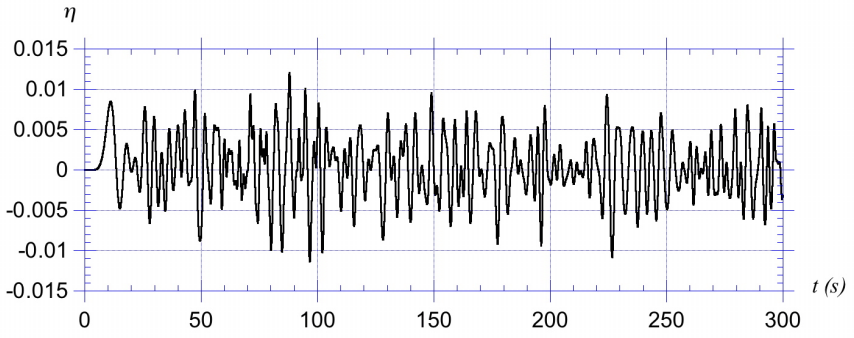

Figure 11: Typical irregular waves generated in the 2D-NWT based on a specified JONSWAP spectrum [39].

tion leading to sparse matrices, and a MPI parallel implementation) and in its generation of well controlled irregular wave sea states. Figure 11 shows for instance a time series of surface elevation simulated in the model, for irregular waves generated using a flap wavemaker motion, based on a specified JONSWAP energy spectrum. A few iterations are performed in the generation, until the target spectrum is satisfactorily created in the NWT. Once the development and implementation of the full hybrid model are complete, including the possibility of running the model on very large computer clusters, such irregular wave forcing could be used to perform long term simulations of wave-induced sediment transport and resulting scouring or burial of a bottom obstacle. The latter aspect of moving bed is still being developed and validated.

In the following, we just present typical results of flow and sediment transport induced over a flat bottom, around a 75% buried circular cylinder of 8.4 cm radius, in a sandy seabed ($d_{50} = 0.2$ mm, $\rho_s = 2,650$ kg/m^3, $w_s = 0.026$ m/s, $k_s = 1$ mm) by a (nonlinear) periodic wave of height $H = 0.12$ m and period $T = 0..84$ s, in water depth $d = 0.8$ m (these are in fact laboratory scales of earlier laboratory experiments performed with a moving sandy bed [61, 62]). Similar simulations were performed with the earlier version of the model [43], and are repeated here in the new hybrid model implementation.

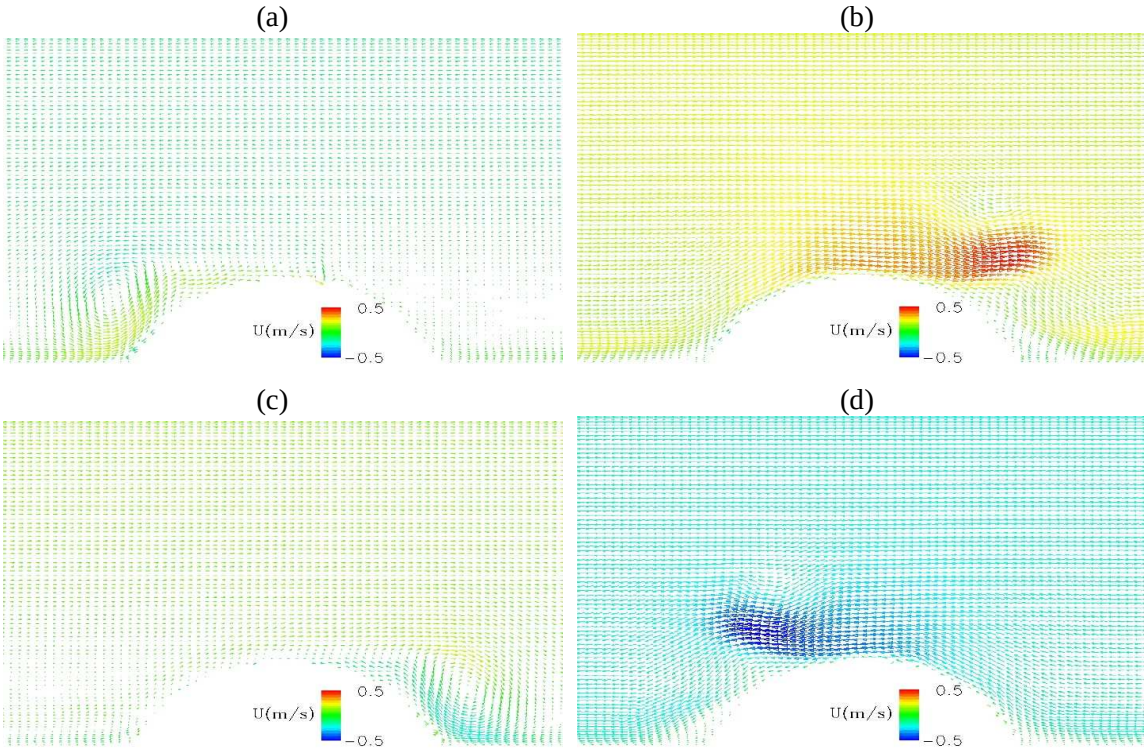

Figure 12: Typical wave-induced (mean) velocity fields ($y = 0$) ($U_i = U_i^I + U_i^P$) computed in the NS-LES model for periodic wave forcing, around a 75% buried circular cylinder. (a)-(d) denote various stages of the flow during one wave period.

NWT discretization. Typical free surface discretization (on Γ_f) in the 2D-NWT usually have at least 20 nodes per dominant wavelength (e.g., Fig. 1). Lateral boundaries (Γ_w and Γ_p) are typically discretized with only 7-11 nodes. Bottom discretization (on Γ_b) are usually a little coarser than on the free surface, but horizontal node spacing (Δx) is reduced on the bottom under the NS-LES domain, in order to further increase the accuracy of the integrals used to compute internal fields in the BEM solution . Adaptive integrations, with up to 2^4 subdivisions, are performed within 4 nodes of any corner of the BEM domain, and for all elements located directly under the NS domain, where points at which internal velocities and their gradients are calculated and used for model coupling are specified. Initial time steps are selected based on the free surface node spacing, to satisfy the optimal mesh Courant number. Time step is subsequently automatically adjusted as a function of the minimum distance between nodes on the free surface in order to satisfy the Courant condition. Typical CPU times in the NWT are less than one second per time step on a desktop computer.

In this applications, the NWT was run without bottom friction, and with no regridding applied on the free surface, because no long term computations were run for simple periodic waves, as only a few (10) periods of wave forcing were used in the NS-LES domain. Longer term computations, for instance with irregular waves (Fig. 11) and/or moving bottom (such as migrating ripples), would require to include bottom friction dissipation and regridding the free surface (see [61, 62]). An absorbing beach AB and an absorbing piston AP (Fig. 1) are specified in order to damp incident wave energy and eliminate (or reduce) wave reflection at the NWT extremity.

NS-LES model discretization. The NS-LES model domain dimensions are 0.3 m long by 0.173 m high by 0.0125 m wide (Fig. 7a). For the partially buried obstacle, the bottom is flat in the streamwise direction to either side of a central bump, represented by a 75% buried cylinder of

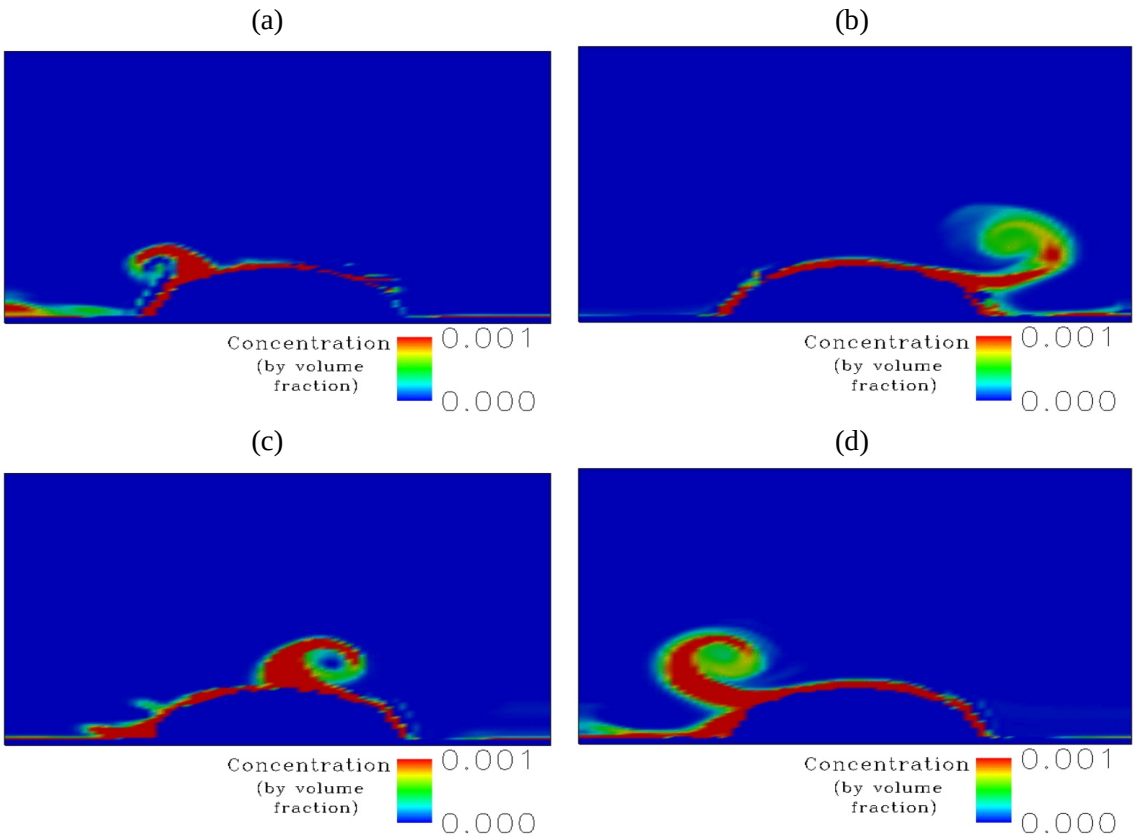

Figure 13: Typical wave-induced (mean) sediment concentration ($y = 0$) ($\overline{C}$) computed in the NS-LES model for periodic wave forcing, around a 75% buried circular cylinder. (a)-(d) denote various stages of the flow during one wave period (see Fig. 12).

radius 0.084 m, whose axis runs in the spanwise direction. The NS-LES model is discretized by 82 x 98 x16 grid points. Hence, 82x98 = 8,036 points are used in each vertical plane of the 3D NS-LES domain. The immersed boundary is located above the actual grid boundary so that the total flow domain height is 0.17 m (discretized by 95 points in the vertical direction over the flat regions). The obstacle protrudes a vertical distance of 0.042 m into the flow. The wave forcing is two dimensional, as is the bed and, based on our previous work [43], the main structure of the vortices in the vertical plane is not significantly influenced by cross-stream resolution in channel flows. Accordingly, we used a smaller number of of cross-stream grid points, assuming that while the flow will not be as well resolved in that direction, the results in the vertical plane are not noticeably impacted. No change in the model or set-up, however, is required to increase the cross-stream resolution, but the computer time required increases rapidly as one does that. [Such cases with finer lateral discretization will be run in the near future, with the newly developed MPI parallel version of the code, on large computer clusters.]

For the coupled simulations with a periodic wave flow, wave forcing is computed in the NWT at the grid cell centers of the the fixed embedded NS-LES domain. Thus, the NWT provides the far field velocities and free-surface wave forcing throughout most of the domain Ω, while the embedded NS solution provides a well-resolved description of the wave boundary layer within its domain, with no slip enforced at the bed. Wave generation is ramped-up over three periods in the NWT and computations are performed until a quasi-steady regime is reached. This usually takes 10 wave periods or so. Internal velocity fields are then calculated in the NWT to both initialize and subsequently force the NS-LES model. There is no NWT forcing in the transverse direction for

this 2D flow, but turbulent fluctuations will carry momentum laterally to the main flow direction, in the NS-LES model.

Examples of velocity and sediment concentration results computed in the NS-LES model around the cylinder are shown in Figs. 12 and 13, for the eleventh period of run time (the first 10 periods are model ramp-up). In this case, the suspended sediment concentration field was initialized as a function of the bottom shear stress at the end of the tenth period. Results are shown in a vertical plane at $y = 0$. [Bedload was not computed for this initial illustration of our coupled model computations.]

Characteristic of all boundary layers, velocity profiles shown in Fig. 12 tend to zero along the bed, with larger near-bed velocities surrounding the crest of the cylinder. Shear layers form in the lee of the mine during wave phases where the velocity tapers off from its maximum value, as would be expected for a typical oscillatory flow case. As the flow slows enough so that it is about half its maximum value, some of the near-bed velocities reverse and form what looks to be the beginning of a typical lee vortex. However, as the flow slows to zero, the pressure gradient distribution on the cylinder from the NWT acts to intensify the flow in the direction *down the slope*. This jet of fluid is now moving in the direction opposite to the new flow direction. After the flow switches direction, this near-bed jet of fluid, which opposes the new main flow direction, rolls up into a spanwise vortex on the *stoss* side of the cylinder.

As expected, the sediment transport patterns in Fig. 13 follow the flow field very closely. However, the entrainment patterns differ significantly because the boundary condition along the cylinder enforces the condition $C = 0$. Strictly, this is only a first approximation to the correct boundary condition, which would allow for deposition and subsequent pickup on the obstacle boundary Γ_b. For the case studied here, this approximate boundary condition may have contributed to oscillations in the concentration profiles, which eventually lead to somewhat unrealistic behavior in the sediment concentration field. In general, sediment is picked up where the shear stresses are greater than critical along the flat bottom regions both upstream and downstream of the cylinder. It is then oscillated back and forth over the mine due to the action of the flow. More details and discussions of such flow and sediment patterns can be found in [43].

5. CONCLUSIONS

The illustrations and applications of hybrid model coupling methodologies presented here show that, by seamlessly combining and integrating the best features of different fluid models, with different (but relevant) "physics" (and/or spatial and temporal scales), in various parts of the fluid domain, one can achieve both an accurate and efficient solution of complex free surface flow problems, including in the presence of structures and with complex seabed dynamics.

While the presented applications were only aimed at both illustrating and validating model features, and hence were of limited complexity and size, the MPI parallel implementation of the models on very large computer clusters makes it possible simulating problems of increasingly practical interest and relevance to various fields of engineering. Such tools can also be used to investigate and gain insight into complex physical processes involving, e.g., turbulent boundary layer flows, the interaction of those with rigid structures, and/or a moving bed, and the sediment transport that might result.

While the present paper was devoted to the coupling of FNPF-NWT and a (submerged) NS-LES model, which have been spearheaded by Grilli and co-workers, the same hybrid approach can of course be (and is being) used to couple other types of models, such as FNPF/HOS or NWT models with NS models around surface piercing fixed or floating structures, or long wave (e.g., BM) model with NS-VOF or SPH models; this currently being researched by various other groups.

ACKNOWLEDGEMENT

The author is appreciative of the support provided under Grants N00014-00-1-0440 by the U.S.A. Office of Naval Research, Coastal Dynamics Program and N00014-05-1-0068 of the Office of Naval Research, Coastal Geosciences Division, Mine Burial Burial Program (code 321CG) [Dr. Thomas Drake, Program Officer].

REFERENCES

[1] Abadie, S., Grilli, S.T. and Glockner, S. (2006). A coupled numerical model for tsunamis generated by subaerial and submarine mass failures. In *Proc. 30th Intl. Conf. on Coastal Engng.* (ICCE30, San Diego, California, September 2006), pps. 1420-1431.

[2] Abadie, S., Morichon, D., Grilli, S.T. and Glockner, S. (2008). VOF/Navier-Stokes numerical modeling of surface waves generated by subaerial landslides. *La Houille Blanche*, **1** (Feb. 2008), 21-26.

[3] Alessandrini, B. (2007). Thése d'Habilitation en Vue de Diriger les Recherches. *Ecole Centrale de Nantes*, Nantes, PhD thesis.

[4] Biausser B., S.T. Grilli, Fraunie P. and Marcer, R. (2004) Numerical analysis of the internal kinematics and dynamics of three-dimensional breaking waves on slopes. *Intl. J. Offshore and Polar Engng.*, **14**(4), 247-256.

[5] Boo, S. Y., Kim, C. H. and Kim, M. H. (1994). A numerical wave tank for nonlinear irregular waves by three-dimensional higher-order boundary element method. *Intl J. Offshore and Polar Engng*, 265–272.

[6] Bonnefoy F., Le Touze D. and Ferrant P. (2004). Generation of fully-nonlinear prescribed wave fields using a high-order spectral method, In *Proc. 14th Offshore and Polar Engng. Conf.* (ISOPE 2004, Toulon, France), 257–263, 2004.

[7] Brandini, C. and Grilli, S. T. (2001). Modeling of freak wave generation in a three-dimensional NWT. In *Proc. 11th Intl Offshore and Polar Engng Conf.*, Stavanger, Norway, pp. 124–131, ISOPE.

[8] Brandini, C. and Grilli, S. T. (2002). Three-dimensional wave focusing in fully nonlinear wave models. In *Proc. 4th Intl Symp. on Ocean Wave Measurement and Analysis* (San Francisco, USA), 1102–1111, ASCE.

[9] Broeze, J. (1993). Numerical modelling of nonlinear free surface waves with a three-dimensional panel method. PhD thesis, University of Twente, Enschede, The Netherlands.

[10] Broeze, J., Van Daalen, E. F. G. and Zandbergen, P. J. (1993). A three-dimensional panel method for nonlinear free surface waves on vector computers. *Comput. Mech.*, **13**, 12–28.

[11] Celebi, M. S., Kim, M. H. and Beck, R. F. (1998). Fully nonlinear three-dimensional numerical wave tank simulations. *J. Ship. Res.*, **42**, 33–45.

[12] Chen, G., Kharif, C., Zaleski, S. and Li, J. (1999). Two-dimensional Navier–Stokes simulation of breaking waves. *Phys. Fluids*, **11**, 121–133.

[13] Christensen, E. D. and Deigaard, R. (2001). Large eddy simulation of breaking waves. *Coastal Engng.*, **42**, 53-86.

[14] Clamond, D., Fructus, D., Grue, J. and Kristiansen, O. (2005). An efficient model for three-dimensional surface wave simulations. Part II: Generation and absorption. *J. Comput. Phys.*, **205**, 686–705.

[15] Clément, A. (1996), Coupling of Two Absorbing Boundary Conditions for 2D Time-domain Simulations of Free Surface Gravity Waves. *J. Comp. Phys.,* **126,** 139-151.

[16] Cointe, R. (1990). Numerical simulation of a wave channel. *Engng Anal. Bound. Elem.*, **7**, 167–177.

[17] Corte, C. and Grilli S.T. (2006). Numerical Modeling of Extreme Wave Slamming on Cylindrical Offshore Support Structures. In *Proc. 16th Offshore and Polar Engng. Conf.* (ISOPE06, San Francisco, California, June 2006), **3**, 394-401.

[18] Cui, A. and R.L. Street (2001). Large-eddy simulation of turbulent rotating convective flow development, *J. Fluid Mechanics*, **447**, 5384.

[19] Dalrymple, R.A., Grilli, S.T. and J.T. Kirby (2006). Tsunamis and challenges for accurate modeling. *Oceanography*, **19**(1), 142-151.

[20] Dalrymple, R.A. and Rogers, B.D. (2006). Numerical Modeling of Water Waves with the SPH Method. *Coastal Engineering*, **53**(2-3), 141-147.

[21] Day, S. J., P. Watts, S. T. Grilli and Kirby, J.T. (2005). Mechanical Models of the 1975 Kalapana, Hawaii Earthquake and Tsunami. *Marine Geology*, **215**(1-2), 59-92.

[22] Dias F., Bridges T (2006). The numerical computation of freely propagating time-dependent irrotational water waves, *Fluid Dyn. Research*, **38**, 803–830.

[23] Dommermuth, D.G. and Yue, D.K.P. (1987). A High Order Spectral Method for the Study of Nonlinear Gravity Waves. *J. Fluid Mech.,* **184,** 267-288.

[24] Dommermuth, D. G., Yue, D. K. P., Lin, W. M., Rapp, R. J., Chan, E. S. and Melville, W. K. (1988). Deep-water plunging breakers: a comparison between potential theory and experiments. *J. Fluid Mech.*, **189**, 423–442.

[25] Ducrozet, G., Bonnefoy, F., Le Touzé, D., and P. Ferrant (2007). 3-D HOS simulations of extreme waves in open seas. *Nat. Hazards Earth Syst. Sci.*, **7**, 109-122.

[26] El Bettah, M., S.T., Grilli, C. Baxter, K. Bollinger, and M. Kravczyk (2008). On the triggering of underwater landslides by earthquakes : a microfluidics modeling and experimental approach. In *Proc. ISOPE 2008 Intl. Conf.* (Vancouver, CA, July 2008), and submitted to *Intl. J. Offshore and Polar Eneng.*.

[27] Enet, F, Grilli, S.T. and Watts, P., (2003). Laboratory Experiments for Tsunamis Generated by Underwater Landslides: Comparison with Numerical Modeling. In *Proc. 13th Offshore and Polar Engng. Conf.* (ISOPE03, Honolulu, USA, May 2003), 372-379.

[28] Enet F. and Grilli S.T. (2005). Tsunami Landslide Generation: Modelling and Experiments. In *Proc. 5th Intl. on Ocean Wave Measurement and Analysis* (WAVES 2005, Madrid, Spain, July 2005), IAHR Publication, paper 88, 10 pps.

[29] Enet, F. (2006). *Tsunami generation by underwater landslides*. Ph.D Dissertation, Department of Ocean Engineering, University of Rhode Island.

[30] Enet, F. and Grilli, S.T. (2007). Experimental Study of Tsunami Generation by Three-dimensional Rigid Underwater Landslides. *J. Waterway Port Coastal and Ocean Engng.*, **133**(6), 442-454.

[31] Ferrant, P. (1996). Simulation of strongly nonlinear wave generation and wave–body interactions using a fully nonlinear MEL model. In *Proc. 21st Symp. on Naval Hydrodynamics*, Trondheim, Norway, pp. 93–108.

[32] Fochesato, C., Dias, F., and Grilli, S.T. (2003). Numerical Model Using the Fast Multipole Algorithm for Nonlinear Three-dimensional Free Surface Waves over Arbitrary Bottom. In *Proc. 13th Offshore and Polar Engng. Conf.* (ISOPE03, Honolulu, USA, May 2003).

[33] Fochesato, C., Grilli, S. and Guyenne P. (2005). Note on non-orthogonality of local curvilinear co-ordinates in a three-dimensional boundary element method. *Intl. J. Numer. Meth. In Fluids*, **48**, 305-324.

[34] Fochesato C. and Dias F. (2006). A fast method for nonlinear three-dimensional free-surface waves, *Proc. Roy. Soc. Lond. A* **462**, 2715–2735.

[35] Fochesato C., Grilli, S.T. and Dias F. (2007). Numerical modeling of extreme rogue waves generated by directional energy focusing. *Wave Motion*, **44**, 395-416.

[36] Fritz, H.M. (2002). Initial Phase of Landslide Generated Impulse Waves. *PhD Dissertation*, Swiss Federal Institute of Technology Zürich.

[37] Fritz, H.M., Hager, W.H. and H.-E. Minor (2004). Near Field Characteristic of Landslide Generated Impulse Waves. *J. Wtrwy, Port, Coast, and Oc. Engrg.*, **130**(6), 287-302.

[38] Fructus, D., Clamond, D., Grue, J. and Kristiansen, O. (2005). An efficient model for three-dimensional surface wave simulations. Part I: Free space problems. *J. Comput. Phys.*, **205**, 665–685.

[39] Greene, N.A. (2008). *Irregular wave generation in a fully nonlinear potential flow numerical wave tank*, Masters Thesis, University of Rhode Island.

[40] Greengard L. (1988). *The Rapid Evaluation of Potential Fields in Particle Systems*, MIT Press, Cambridge, MA, 1988.

[41] Greengard L. and Rokhlin V. (1987). A fast algorithm for particle simulations. *J. Comput. Phys.*, **73**, 325–348.

[42] Gilbert R.W., Grilli S.T., Zedler E.A., and Street R.L. (2005). Modelling of Wave-Driven Sediment Transport in the Shoaling Zone. In *Proc. 5th Intl. Symp. on Ocean Wave Measurement and Analysis* (WAVES 2005, Madrid, Spain, July 2005), IAHR Publication, paper 121, 10 pps.

[43] Gilbert R.W., Zedler E.A., Grilli S.T., and Street R.L. (2007). Progress on Nonlinear-Wave-Forced Sediment Transport Simulation. *IEEE J. of Oceanic Engng.*, **32**(1), 236-248.

[44] Grilli, S.T. (1997). Fully Nonlinear Potential Flow Models used for Long Wave Runup Prediction. Chapter in *Long-Wave Runup Models*, (eds. H. Yeh, P. Liu, and C. Synolakis), pps. 116-180. World Scientific Publishing, Singapore.

[45] Grilli, S.T., Dias, F., Guyenne, P., Fochesato, C. and F. Enet (2008). Progress In Fully Nonlinear Potential Flow Modeling Of 3D Extreme Ocean Waves. Chapter in *Advances in Numerical Simulation of Nonlinear Water Waves* (Series in Advances in Coastal and Ocean Engineering). World Scientific Publishing Co.Pte.Ltd., 55 pps. (in press). http://www.oce.uri.edu/∼grilli/Grilli-etal-chapter.pdf

[46] Grilli, S.T., Gilbert, R.W., Lubin, P., Vincent, S., Legendre, D., Duvam, M., Kimmoun, O., Branger, H., Devrard, D., Fraunie, P., Abadie, S. (2004). Numerical modeling and experiments for solitary wave shoaling and breaking over a sloping beach. In *Proc. 14th Offshore and Polar Engng. Conf.* (ISOPE04, Toulon, France, May 2004), 306-312.

[47] Grilli, S.T., Guyenne, P. and F. Dias (2001). A fully nonlinear model for three-dimensional overturning waves over arbitrary bottom. *Intl. J. Numerical Methods in Fluids*, **35**(7), 829-867.

[48] Grilli, S.T., Harris, J. and Greene, N. (2008). Modeling of Wave-induced Sediment Transport in the Shoaling Zone in the Presence of Bottom Obstacle. Extended abstract in *31st Intl. Coastal Engineering Conference* (ICCE 2008, Hamburg, Germany) (full paper to appear).

[49] Grilli, S.T. and Horrillo, J. (1997). Numerical Generation and Absorption of Fully Nonlinear Periodic Waves. *J. Engng. Mech.*, **123**(10), 1060-1069.

[50] Grilli, S.T. and Horrillo J. (1997). Fully Nonlinear Properties of Periodic Waves Shoaling over Mild Slopes. In *Proc. 25th Intl. Conf. on Coastal Engng.* (ICCE25, Orlando, USA, September 96), Vol. 1, pps. 717-730. ASCE Edition.

[51] Grilli, S.T., Ioualalen, M, Asavanant, J., Shi, F., Kirby, J. and Watts, P. (2007). Source Constraints and Model Simulation of the December 26, 2004 Indian Ocean Tsunami. *J. Waterway Port Coastal and Ocean Engng.*, **133**(6), 414-428.

[52] Grilli, S.T., Skourup, J. and Svendsen, I.A. (1988). The Modeling of Highly Nonlinear Waves : A Step Toward the Numerical Wave Tank. In *Proc. 10th Intl. Conf. on Boundary Elements* (BEM10, Southampton, England, September 88) (ed. C.A. Brebbia) Vol. 1, pp. 549-564. Computational Mechanics Publication. Springer-Verlag, Berlin.(invited paper).

[53] Grilli, S.T., Skourup, J. and Svendsen, I.A. (1989). An Efficient Boundary Element Method for Nonlinear Water Waves. *Engng. Anal. Bound. Elem.*, **6**(2), 97-107.

[54] Grilli, S.T. and Subramanya, R. (1994). Quasi-singular Integrations in the Modelling of Nonlinear Water Waves. *Engineering Analysis with Boundary Elements*, **13**(2), 181-191.

[55] Grilli, S.T. and Subramanya, R. (1996). Numerical Modeling of Wave Breaking Induced by Fixed or Moving Boundaries. *Computational Mech.*, **17**, 374-391.

[56] Grilli, S., Subramanya, R., Svendsen, I.A. and Veeramony, J. (1994). Shoaling of Solitary Waves on Plane Beaches. *J. Waterway Port Coastal and Ocean Engineering*, **120**(6), 609-628.

[57] Grilli, S.T. and Svendsen, I.A. (1990). Corner Problems and Global Accuracy in the Boundary Element Solution of Nonlinear Wave Flows. *Engineering Analysis with Boundary Elements*, **7**(4), 178-195.

[58] Grilli, S.T., Svendsen, I.A. and Subramanya, R. (1997). Breaking Criterion and Characteristics for Solitary Waves on Slopes. *J. Waterway Port Coastal and Ocean Engng.*, **123**(3), 102-112.

[59] Grilli, S.T., Svendsen, I.A. and Subramanya, R. (1998). Closure of : Breaking Criterion and Characteristics for Solitary Waves on Slopes. *J. Waterway Port Coastal and Ocean Engineering*, **124**(6), 333-335.

[60] Grilli, S.T., Vogelmann, S. and Watts, P. (2002). Development of a 3D Numerical Wave Tank for modeling tsunami generation by underwater landslides. *Engng. Analysis Boundary Elemt.*, **26**(4), 301-313.

[61] Grilli, S.T., Voropayev, S., Testik, F.Y. and Fernando, H.J.S. (2003). Numerical Modeling and Experiments of Wave Shoaling over Buried Cylinders in Sandy Bottom. In *Proc. 13th Offshore and Polar Engng. Conf.* (ISOPE03, Honolulu, USA, May 2003), 405-412.

[62] Grilli, S.T., Voropayev, S., Testik, F.Y. and Fernando, H.J.S. Numerical modeling and experiments of periodic waves shoaling over semi-buried cylinders in sandy bottom. *J. of Waterway Port Coastal and Ocean ineering* (in revision). http://www.oce.uri.edu/∼grilli/mineASCE.pdf

[63] Grilli, S.T. and Watts, P. (1999). Modeling of waves generated by a moving submerged body. Applications to underwater landslides. *Engng. Analysis Boundary Elemt.*, **23**, 645-656.

[64] Grilli, S.T. and P. Watts. (2005). Tsunami generation by submarine mass failure Part I : Modeling, experimental validation, and sensitivity analysis. *J. Waterway Port Coastal and Ocean Engng.*, **131**(6), 283-297.

[65] Guignard, S., Grilli, S.T., Marcer, R. and Rey, V. (1999). Computation of shoaling and breaking waves in nearshore areas by the coupling of BEM and VOF methods. In *Proc. 9th Offshore and Polar Engng. Conf.* (ISOPE99, Brest, France, May 1999), Vol. III, 304-309.

[66] Guignard, S. and S.T., Grilli (2001). Modeling of shoaling and breaking waves in a 2D-NWT by using a spilling breaker model. In *Proc. 11th Offshore and Polar Engng. Conf.* (ISOPE01, Stavanger, Norway, June 2001), Vol III, 116-123.

[67] Guignard, S. and S.T., Grilli (2002). Implementation and validation of a breaker model in a fully nonlinear wave propagation model. In *Proc. 4th Intl. Symp. on Ocean Wave Measurement and Analysis* (WAVES 2001, San Francisco, USA, Sept. 2001) 1,012-1,021, ASCE Publication.

[68] Guyenne, P. and Grilli, S.T. (2003). Computations of 3D Overturning Waves in Shallow Water. In *Proc. 13th Offshore and Polar Engng. Conf.* (ISOPE03, Honolulu, USA, May 2003), 347-352.

[69] Guyenne, P. and Grilli, S.T. (2006). Numerical study of three-dimensional overturning waves in shallow water. *J. Fluid Mechanics*, **547**, 361-388.

[70] Guyenne, P., Grilli, S. T. and Dias, F. (2000). Numerical modelling of fully nonlinear three-dimensional overturning waves over arbitrary bottom. In *Proc. 27th Intl Conf. on Coastal Engng* (Sydney, Australia), 417–428, ASCE.

[71] Harris, J.C., and Grilli S.T. (2007). Computation of the wavemaking resistance of a Harley surface effect ship. In *Proc. 17th Offshore and Polar Engng. Conf.* (ISOPE07, Lisbon, Portugal, July 2007), 3732-3739.

[72] Helluy Ph., Golay F., Caltagirone J.-P., Lubin P., Vincent S., Drevard D., Marcer R., Seguin N., Grilli S., Lesage A.-C. and Dervieux A. (2005). Numerical simulations of wave breaking. *Math. Modeling and Numer. Analys.*, **39**(3), 591-607.

[73] Ioualalen, M. , Asavanant, J., Kaewbanjak, N., Grilli, S.T., Kirby, J.T. and P. Watts (2007). Modeling the 26th December 2004 Indian Ocean tsunami: Case study of impact in Thailand. *J. Geophys. Res.*, **112**, C07024.

[74] Jensen, B. L. , B. M. Sumer, and J. Fredsoe (1989). Turbulent oscillatory boundary layers at high Reynolds numbers. *J. Fluid Mechanics*, **206**, 265297.

[75] Kim, K., A. I. Sirviente, and R. F. Beck. (2005). The complimentary RANS equations for the simulation of viscous flows. *Intl. J. Numer. Meth. Fluids*, **48**, 119–229.

[76] Korsmeyer F.T., Yue D.K.P. and Nabors K. (1993). Multipole-Accelerated Preconditioned Iterative Methods for Three-Dimensional Potential Problems. Presented at *15th Intl. Conf. on Boundary Element*, Worcester, MA.

[77] Lachaume, C., Biausser, B., Grilli, S.T., Fraunie, P. and Guignard, S. (2003). Modeling of breaking and post-breaking waves on slopes by coupling of BEM and VOF methods. In *Proc. 13th Offshore and Polar Engng. Conf.* (ISOPE03, Honolulu, USA, May 2003), 353-359.

[78] Leonard, B. P. (1979). A stable and accurate convective modelling procedure based on quadratic upstream interpolation. *Comp. Meth. in Applied Mechanics and Engng.*, **19**, 59–98.

[79] Leonard, B. P. (1988). Simple high accuracy resolution program for convective modeling of discontinuities.*Intl. J. Numerical Meth. in Fluids*, **8**, 1291–1318.

[80] Lin, P. and Liu, P. L.-F. (1998). A numerical study of breaking waves in the surf zone. *J. Fluid Mech.*, **359**, 239–264.

[81] Liu, P. L.-F., Wu, T.-R., Raichlen, F., Synolakis, C.E. and Borrero, J.C., (2005). Runup and rundown generated by three-dimensional sliding masses. *J. Fluid Mech.*, **536**, 107-144.

[82] Longuet-Higgins, M. S. and Cokelet, E. D. (1976). The deformation of steep surface waves on water. I. A numerical method of computation. *Proc. R. Soc. Lond.*, A **350**, 1–26.

[83] Lubin, P. (2004). *Large Eddy Simulations of plunging breaking waves*. Ph.D Dissertation, University of Bordeaux I, France.

[84] New, A. L., McIver, P. and Peregrine, D. H. (1985). Computations of overturning waves. *J. Fluid Mech.*, **150**, 233–251.

[85] Nakayama, A. and Noda, H. and Maeda, K. (2004). Similarity of instantaneous and filtered velocity fields in t he near wall region of zero-pressure gradient boundary layer. *Fluid Dynamics Research*, **35**, 299–321,

[86] Nishimura N. (2002). Fast multipole accelerated boundary integral equation methods. *Appl. Mech. Rev.*, **55**, 299–324.

[87] Rokhlin V. (1985). Rapid solution of integral equations of classical potential theory. *J. Comput. Phys.* **60**, 187–207.

[88] Romate, J.E. (1989). *The Numerical Simulation of Nonlinear Gravity Waves in Three Dimensions using a Higher Order Panel Method.* Ph.D. Dissertation. Department of Applied Mathematics, University of Twente, The Netherland, 1989.

[89] Scorpio S. and Beck F. (1996). A Multipole Accelerated Desingularized Method for Computing Nonlinear Wave Forces on Bodies. Presented at *15th Intl. Conf. Offshore Mech. Arctic Engng.* (Florence, Italy).

[90] Skyner, D. J. (1996). A comparison of numerical predictions and experimental measurements of the internal kinematics of a deep-water plunging wave. *J. Fluid Mech.*, **315**, 51–64.

[91] Sung H.G. and Grilli S.T. (2006). Combined Eulerian-Lagrangian or Pseudo-Lagrangian, Descriptions of Waves Caused by an Advancing Free Surface Disturbance. In *Proc. 16th Offshore and Polar Engng. Conf.* (ISOPE06, San Francisco, California, June 2006), **3**, 487-494.

[92] Sung, H.G. and Grilli, S.T. (2008). BEM Computations of 3D Fully Nonlinear Free Surface Flows Caused by Advancing Surface Disturbances. *Intl. J. Offshore and Polar Engng.* (accepted). http://www.oce.uri.edu/∼grilli/SungGIJOPE2007.pdf

[93] Tappin, D.R., Watts, P., Grilli, S.T. (2008). The Papua New Guinea tsunami of 1998: anatomy of a catastrophic event. *Natural Hazards and Earth Syst. Sc.*, **8**, 243-266.

[94] Tanaka, M. (1986). The stability of solitary waves. *Phys. Fluids*, **29**, 650–655.

[95] Tseng, Y. H. and J. H. Ferziger (2003). A ghost-cell immersed boundary method for flow in complex geometry. *J. of Computational Physics*, **192**, 593–623

[96] van Rijn, L. C., (1984). Sediment transport, Part I: bed load transport. *J. Hydraulic Engineering*, **110**, (10), 14311456.

[97] van Rijn, L. C., (1993). *Principles of Sediment Transport in Rivers, Estuaries and Coastal Seas.* Aqua Publications, Amsterdam, The Netherlands.

[98] Vinje, T. and Brevig, P. (1981). Numerical simulation of breaking waves. *Adv. Water Resour.*, **4**, 77–82.

[99] Watts, P. and Grilli, S.T., (2003). Tsunami Generation by Deformable Underwater Landslides. In *Proc. 13th Offshore and Polar Engng. Conf.* (ISOPE03, Honolulu, USA, May 2003), 364-371.

[100] Watts, P., S. T. Grilli, J. T. Kirby, G. J. Fryer, and Tappin, D. R. (2003). Landslide tsunami case studies using a Boussinesq model and a fully nonlinear tsunami generation model. *Natural Hazards and Earth Syst. Sc.*, **3**, 391-402.

[101] Watts, P., Grilli, S.T., Tappin D., and Fryer, G.J. (2005). Tsunami generation by submarine mass failure Part II : Predictive Equations and case studies. *J. Waterway Port Coastal and Ocean Engng.*, **131**(6), 298-310.

[102] Wei, J., Kirby, J.T, Grilli, S.T. and Subramanya, R. (1995). A Fully Nonlinear Boussinesq Model for Surface Waves. Part1. Highly Nonlinear Unsteady Waves.*J. Fluid Mech.*, **294**, 71-92.

[103] Xü, H. and Yue, D. K. P. (1992). Computations of fully nonlinear three-dimensional water waves. In *Proc. 19th Symp. on Naval Hydrodynamics* (Seoul, Korea).

[104] Xue, M., Xü, H., Liu, Y. and Yue, D. K. P. (2001). Computations of fully nonlinear three-dimensional wave–wave and wave–body interactions. Part 1. Dynamics of steep three-dimensional waves. *J. Fluid Mech.*, **438**, 11–39.

[105] Yim, S.C. , H. Lin and K. Tanizawa (2007). Fully-Nonlinear Potential Flow Model Analysis of Stochastic Responses of an Experimental Fluid-Structure Interaction System. *Offshore Mech. and Arctic Engn., ASME*, **129**, 9-20.

[106] Yim, S.C. , H. Lin, D.C. Robinson and K. Tanizawa (2008). Predictive Capability of a Fully-Nonlinear Potential Flow Model of a Fluid-Structure Interaction System. *Offshore Mech. and Arctic Engn., ASME*, Manuscript No.OMAE-20056-1101 (in press).

[107] Yim, S.C. , D. Yuk, A. Panizzo, M. Di Risio and P.L-F. Liu (2008). Numerical Simulations of Wave Generation by a Vertical Plunger Using RANS and SPH Models. *J. Waterway, Port, Coastal and Ocean Engng., ASCE* (in press).

[108] Zang, Y. (1993). *On the development of tools for the simulation of geophysical flows.* Ph.D. dissertation, Stanford University.

[109] Zang, Y., Street, R. L. and Koseff, J. R. (1994). A non-staggered grid, fractional step method for time-dependent incompressible Navier Stokes equations in curvilinear coordinates *J. of Computational Physics*, **114**, 18–33.